

**Analysis of magnetic anisotropy and the role of intermolecular interactions in switching SMM behaviour in a family of Co(II)-Y(III) dinuclear complexes with easy-plane anisotropy: A magneto-structural and theoretical study**

María A. Palacios,<sup>⊥</sup> Joscha Nehr Korn,<sup>†,§</sup> Elizaveta A. Sutura<sup>‡</sup>, Eliseo Ruiz<sup>#,\*</sup>, Silvia Gómez-Coca,<sup>#</sup> Karsten Holldack,<sup>§</sup> Alexander Schnegg<sup>§</sup>, J. Krzystek,<sup>¶</sup> José. M. Moreno,<sup>⊥</sup> Enrique Colacio<sup>⊥,\*</sup>

<sup>⊥</sup>Departamento de Química Inorgánica, Facultad de Ciencias, Universidad de Granada, 18071 Granada, Spain

<sup>†</sup>Department of Chemistry, Box 351700, University of Washington, Seattle, Washington 98195, USA

<sup>§</sup> Berlin Joint EPR Lab, Institute for Nanospectroscopy, Helmholtz-Zentrum Berlin für Materialien und Energie, Kekuléstraße 5, 12489 Berlin, Germany

<sup>‡</sup> Novosibirsk State University, Pirogova str.2, 630090, Novosibirsk, Russia

<sup>#</sup> Departament de Química Inorgànica and Institut de Recerca de Química Teòrica i Computacional, Universitat de Barcelona, Diagonal 645, Barcelona E-08028, Spain

<sup>¶</sup> National High Magnetic Field Laboratory, Florida State University, Tallahassee, Florida 32310, USA

## Abstract

Three new closely related  $\text{Co}^{\text{II}}\text{Y}^{\text{III}}$  complexes of general formula  $[\text{Co}(\mu\text{-L})(\mu\text{-X})\text{Y}(\text{NO}_3)_2]$  ( $\text{X}^- = \text{NO}_3^-$ , **1**, benzoate, **2** and 9-anthracenecarboxylato, **3**) have been prepared with the compartmental ligand  $\text{N,N',N''}$ -trimethyl- $\text{N,N''}$ -bis(2-hydroxy-3-methoxy-5-methylbenzyl)diethylenetriamine ( $\text{H}_2\text{L}$ ). In these complexes  $\text{Co}^{\text{II}}$  and  $\text{Y}^{\text{III}}$  are triply bridged by two phenoxide groups pertaining to the dideprotonated ligand ( $\text{L}^{2-}$ ) and one ancillary anion  $\text{X}^-$ . The change of the ancillary bridging group connecting  $\text{Co}^{\text{II}}$  and  $\text{Y}^{\text{III}}$  ions induces small differences in the trigonally distorted  $\text{CoN}_3\text{O}_3$  coordination sphere with a concomitant tuning of the magnetic anisotropy and intermolecular interactions. Dc-magnetic, HFEPR and FD-FT THz-EPR measurements and *ab initio* theoretical calculations demonstrate that  $\text{Co}^{\text{II}}$  ions in compounds **1-3** have large and positive  $D$  values ( $\sim 50 \text{ cm}^{-1}$ ). Moreover, it has been established that the  $D$  values decrease with increasing the distortion of the  $\text{Co}^{\text{II}}$  coordination sphere. Dynamic ac magnetic susceptibility measurements indicate that compound **1** exhibits field SMMs behaviour, whereas compound **2** and **3** only display this behaviour when are magnetically diluted with diamagnetic  $\text{Zn}^{\text{II}}$  ( $\text{Zn}/\text{Co} = 1/10$ ). The dynamic properties of this family of complexes has been explained on the basis of the existence/absence of large intermolecular interactions, which seems to switch off/on the field induced SIM behaviour. Field and temperature dependence of the relaxation times indicate the prevalence of the Raman process in all these complexes above approximately 3 K.

## Introduction

Nowadays, the field of Molecular Magnetism based on coordination compounds focuses its research attention on systems exhibiting sophisticated magnetic properties such as Single-Molecule Magnets (SMMs).<sup>1</sup> These nanomagnets can function as single-domain

magnetic nanoparticles but show some advantages over classical magnetic nanoparticles, including reproducibility, monodispersity, magnetic properties that can be modulated by typical chemistry methods, solubility that allows the deposition and grafting on surfaces, among others.<sup>1a</sup> SMMs straddle the quantum/classical boundary as they display magnetic hysteresis below the so-called blocking temperature ( $T_B$ ), a classical property, as well as quantum properties such as quantum tunneling of the magnetization (QTM) and quantum phase interference.<sup>1</sup> These unique properties make them good candidates for potential future applications, among other areas, in ultra-high density magnetic information storage,<sup>2</sup> magneto-optics<sup>3</sup>, molecular spintronics,<sup>1c, 4</sup> and as qubits for quantum computing at molecular level.<sup>1c,5</sup> The ultimate aim of the vast research activity in SMMs is the integration of these systems in nanosize-devices. The SMM behavior is tied to the existence of an energy barrier ( $U$ ) that allows blocking the molecular magnetization either parallel or antiparallel to the magnetic field when the polarizing field is removed below ( $T_B$ ), so that slow relaxation of the magnetization is observed. In principle, the larger the  $U$  value, the higher the temperature at which the SMM behavior is observed, which results in a parallel increase of the relaxation time. For transition metal clusters, the height of the energy barrier can be computed using the expressions  $U = |D|(S_T - 1/4)$  and  $|D|S_T$  for half-integer and integer spin values, respectively, which are connected with the ground state zero-field splitting.<sup>1a</sup> Taking into account this, a strategy to enhance  $U$  would be that of increasing the spin multiplicity of the ground state ( $S_T$ ) and/or the easy-axis (or Ising-type) magnetic anisotropy of the whole molecule ( $D < 0$ ). However, experimental results have shown that both parameters are correlated, so that when  $S_T$  is very large (often observed for high nuclearity clusters),  $D$  tends to be low,<sup>6</sup> so that the increase of  $U$  by increasing simultaneously  $S_T$  and  $D$  is a very difficult task. Moreover, theoretical calculations<sup>7</sup> have

shown that  $U$  is almost independent of  $S$ . As a consequence of the above considerations, the research in this field has targeted mononuclear metal complexes with large anisotropy, containing either transition metal ions with significant first order orbital angular momentum, such as  $\text{Co}^{\text{II}}$ ,  $\text{Fe}^{\text{II}}$  and  $\text{Fe}^{\text{I}}$  or very anisotropic lanthanide ions, particularly the  $\text{Dy}^{\text{III}}$  ion. This together with the fact that mononuclear species can exhibit larger anisotropies than their polynuclear counterparts (as indicated above, the anisotropy of the entire molecule is very hard to control in polynuclear complexes and generally low  $D$  values are observed), has fuelled the search on mononuclear SMMs, also called single-ion magnets (SIMs).<sup>1c,8</sup> Among them, mononuclear complexes containing  $\text{Co}^{\text{II}}$  ( $S = 3/2$ ) are attracting great interest as SIMs because for Kramers ions, in absence of magnetic field, neither direct phonon-induced nor QTM transitions between the states of the ground doublet can be induced by the modulation of the crystal field.<sup>9</sup> The absence of fast QTM favors the observation of thermally activated relaxation and Raman processes. Nevertheless, the splitting of the doublet states arising from first order Zeeman interactions induced by a transversal magnetic field can activate direct and QTM processes. The transversal magnetic field can arise from both internal hyperfine interactions (electronuclear spin entanglement) and intermolecular dipolar interactions.<sup>1</sup> In order to eliminate the latter interactions, magnetically diluted complexes prepared by cocrystalization with an isostructural diamagnetic compound can be employed.<sup>9,10</sup> In the case of the  $\text{Co}^{\text{II}}$ -SIMs,  $\text{Zn}^{\text{II}}$  is generally used for such a magnetic dilution process.<sup>9,10</sup> It is worth noting that SIM behaviour has been observed for  $\text{Co}^{\text{II}}$  complexes with both  $D > 0$  and  $D < 0$ , the former ones being much more numerous than the latter ones (including  $\text{Co}^{\text{II}}\text{Y}^{\text{III}}$  and mixed valence  $\text{Co}^{\text{II}}\text{-Co}^{\text{III}}$  complexes).<sup>8b,c,d</sup> Amid  $\text{Co}^{\text{II}}$  based SIMs, six-coordinated complexes occupy a notable place.<sup>11-12</sup> It should be noted that SIM with  $D < 0$  are limited to a few examples,<sup>11</sup>

which can exhibit SIM behavior under zero applied dc field above 2 K, whereas no SIM behaviour has been observed at zero field for six-coordinated  $\text{Co}^{\text{II}}$  complexes with  $D > 0$  (easy-plane anisotropy).<sup>12</sup> This fact has been justified recently by the acquirement of non-zero magnetic moment by the electronuclear spin states due to the Zeeman interaction.<sup>9</sup>

In this paper, we present three new examples of  $\text{Co}^{\text{II}}\text{Y}^{\text{III}}$  complexes, which can be considered as SIMs as the  $\text{Y}^{\text{III}}$  ion is diamagnetic. These complexes are structurally similar to the dinuclear complex previously reported by us  $[\text{Co}(\mu\text{-L})(\mu\text{-OAc})(\text{NO}_3)_2]$ ,<sup>10</sup> whereas the ancillary acetate bridging group connecting the  $\text{Co}^{\text{II}}$  and  $\text{Y}^{\text{III}}$  ions has been replaced by nitrate, benzoate or 9-anthracene carboxylato bridging groups. In all these complexes the  $\text{Co}^{\text{II}}$  ion is hexacoordinated and  $D$  is expected to be positive. The change of the ancillary bridging group connecting  $\text{Co}^{\text{II}}$  and  $\text{Y}^{\text{III}}$  ions should induce small differences in the  $\text{Co}^{\text{II}}$  coordination sphere with a concomitant tuning of the magnetic anisotropy and intermolecular interactions. The main aim of this work is to disclose how these two factors affect the dynamic of the magnetic relaxation. Interestingly, we will show how magnetic dilution in two of these complexes triggers field-induced SIM behaviour ("SIM hidden behaviour").

## Experimental

### Synthetic procedures

**General Procedures:** Unless stated otherwise, all reactions were conducted in oven-dried glassware in aerobic conditions, with the reagents purchased commercially and used without further purification. The  $\text{H}_2\text{L}$  ligand was prepared as previously reported.<sup>13</sup>

**Synthesis of  $[\text{Co}(\mu\text{-L})(\mu\text{-NO}_3)\text{Y}(\text{NO}_3)_2](1)$ :** To a solution of  $\text{H}_2\text{L}$  (56 mg, 0.125 mmol) in 5 mL MeOH were subsequently added with continuous stirring 36.4 mg (0.125 mmol) of  $\text{Co}(\text{NO}_3)_2 \cdot 6\text{H}_2\text{O}$  and 47.9 mg (0.125 mmol) of  $\text{Y}(\text{NO}_3)_3 \cdot 6\text{H}_2\text{O}$ . The resulting

reddish solution was filtered and allowed to stand at room temperature. After 24-48 hours, well-formed prismatic pink crystals of compound **1** were obtained. Anal. Found: C, 38.75; H, 4.89; N, 10.73. Anal. Calc. for  $C_{25}H_{37}N_6O_{13}CoY$ : C, 38.62; H, 4.80; N, 10.81 9.70 %.

**Synthesis of  $[Co(\mu-L)(\mu-Bz)Y(NO_3)_2](2)$ :** As for complex **1** but also adding 15.3 mg (0.125 mmol) of benzoic acid and 18  $\mu$ L (0.125 mmol) of  $Et_3N$ . The resulting reddish solution was filtered and allowed to stand at room temperature. After 24-48 hours, well-formed prismatic pink crystals of compound **3** were obtained. Anal. Found: C, 45.86; H, 5.00; N, 8.49. Anal. Calc. for  $C_{32}H_{42}N_5O_{12}CoY$ : C, 45.94; H, 5.06; N, 8.37 %.

**Synthesis of  $[Co(\mu-L)(\mu-9-AC)Y(NO_3)_2] \cdot 2CH_3OH \cdot 2H_2O$  (**3**):** As for complex **1** but also adding 27.3 mg (0.125 mmol) of benzoic acid and 18  $\mu$ L (0.125 mmol) of  $Et_3N$ . The resulting reddish solution was filtered and allowed to stand at room temperature. After 24-48 hours, well-formed prismatic pink crystals of compound **2** were obtained. Anal. Found: C, 49.39; H, 5.74; N, 7.34. Calc. for  $C_{42}H_{54}N_5O_{15}CoY$ : C, 49.61; H, 5.35; N, 6.89 %.

**General syntheses of diluted samples 1'-3'**. Analogous to the synthetic method of **1-3** but using a 1:10 Co/Zn ratio, that is 3.63 mg (0.0125 mmol) of  $Co(NO_3)_2 \cdot 6H_2O$  and 37.19 mg (0.125 mmol) of  $Zn(NO_3)_2 \cdot 6H_2O$ . The same method was employed to prepare the diluted complex **3''** with a 5:100 Co/Zn ratio but using 1.81 mg (0.0062 mmol) and 37.19 mg (0.125 mmol) of  $Zn(NO_3)_2 \cdot 6H_2O$ .

### **Physical measurements**

Elemental analyses were carried out at the "Centro de Instrumentacion Cientifica" (University of Granada) on a Fisons-Carlo Erba analyser model EA 1108. IR spectra on powdered samples were recorded with a Thermo Nicolet IR200FTIR using KBr pellets.

Variable-temperature (2–300 K) magnetic susceptibility measurements on polycrystalline samples of **1-3** and **1'-3'** under an applied field of 1000 Oe were carried out with a Quantum Design SQUID MPMS XL-5 device. Alternating-current (ac) susceptibility measurements under different applied static fields were performed using an oscillating ac field of 3.5 Oe and ac frequencies ranging from 1 to 1500 Hz. The experimental susceptibilities were corrected for the sample holder and diamagnetism of the constituent atoms using Pascal's tables. A pellet of the sample cut into very small pieces was placed in the sample holder to prevent any torquing of the microcrystals.

HF-EPR measurements were performed at the NHMFL at several subterahertz frequencies between 50 and 650 GHz and low temperatures on loose powders and pellets, using an instrument described previously in detail<sup>14</sup> with the exception of a Virginia Diodes subterahertz wave source, consisting of a  $13 \pm 1$  GHz frequency generator and a cascade of amplifiers and frequency multipliers. X-Band EPR was performed using a Bruker Elexis 580 X/Q-band EPR spectrometer equipped with a dielectric EN 4118X-MD4 resonator and a cryogen-free ER 4118HV-CF58 FlexLine cooling system. The MW power was 2 mW at the frequency of 9.69 GHz. Modulation amplitude was 0.4 mT at 100 kHz frequency.

Frequency domain Fourier transform THz electron paramagnetic resonance (FD-FT THz-EPR) spectra were measured at the FD-FT THz-EPR experiment at BESSY II, which is described in detail elsewhere.<sup>15,16</sup> An Hg-arc lamp was used as source of broadband unpolarized radiation. Samples were prepared as pressed pellets containing a mixture of the compound under study and PE powder and mounted in the superconducting magnet. For detection purposes a liquid Helium cooled Si bolometer was used. Experimental resolution was 0.5  $\text{cm}^{-1}$ . Due to the fact that magnetic features are often extremely weak in comparison to nonmagnetic absorption in far-IR range,

traditional FT-IR reference methods cannot be used. Absorbance spectra were obtained by using a spectrum measured at a temperature of 30 K as reference spectrum for a spectrum measured at 5 K. Then the absorbance spectrum is obtained as  $A = \log_{10} \left( \frac{I_{ref}}{I_{lowT}} \right)$ , with  $I_{ref}$  the reference spectrum and  $I_{lowT}$  the spectrum measured at a temperature of 5 K. In the energy region investigated in this work several strong non-magnetic absorptions were observed. Therefore it is useful to vary the magnetic field instead of the temperature. For recording Magnetic Field Division Spectra (MDS) the temperature was kept constant at 5 K. The MDS at the magnetic field  $B_0$  is obtained by dividing the spectrum measured at the external magnetic field  $B_0$  by a spectrum measured at the magnetic field  $B_0 + 2$  T. The magnetic field induced shift of an absorptive feature can be observed in the MDS, where a minimum corresponds to stronger absorption at the magnetic field  $B_0$  and a maximum to stronger absorption at the increased magnetic field  $B_0 + 2$  T. Therefore in MDS one can identify magnetic transitions originating from the ground state, due to the low temperature. The field step of 2 T was chosen in accordance with the experimentally observed linewidth of the features. We found that the spectral range is limited at low energies by the characteristic of the used source, which reveal too low radiation intensity below 20  $\text{cm}^{-1}$ . Using instead the very powerful coherent synchrotron radiation of BESSY II running in the low- $\alpha$  mode<sup>17</sup> the spectral range could be increased down to 4  $\text{cm}^{-1}$ . The high-energy limit is due to the z-cut quartz windows of the superconducting magnet.

All simulations and fitting attempts were done using *EasySpin*.<sup>18</sup> Magnetic susceptibility was simulated taking explicitly the applied magnetic field into account. For FD-FT THz-EPR simulations, the recently introduced frequency-domain simulation extension of *EasySpin* including the ability to take into account the fact that the MW radiation can be unpolarized as it was in the experiments presented herein.<sup>19</sup>

## Single-Crystal Structure Determinations.

Suitable crystals of **1-3** and **2'** were mounted on a glass fibre and used for data collection. X-ray diffraction data of **1** and **2** were collected at 110 K using a Bruker AXS SMART APEX CCD diffractometer (Mo K $\alpha$  radiation,  $\lambda = 0.71073$  Å) outfitted with a CCD area-detector and equipped with an Oxford Cryosystems 700 series Cryostream device. Unit-cell parameters were determined and refined on all observed reflections using APEX2 software.<sup>20</sup> Correction for Lorentz polarization and absorption were applied by SAINT and SADABS programs, respectively.<sup>21,22</sup>

Intensity data for compound **3** and **2'** were collected at 100 K on a Agilent Technologies SuperNova diffractometer (mirror-monochromated MoK $\alpha$  radiation,  $\lambda = 0.71076$  Å) equipped with Eos CCD detector. Data collections, unit cell determinations, intensity data integrations, routine corrections for Lorentz and polarization effects and analytical absorption corrections with face indexing were performed using the CrysAlis Pro software package.<sup>23</sup>

The structures were solved by direct methods and refined by the full-matrix least-squares method on  $F^2$  using the SHELX software suite and SHELXL-2014 program.<sup>24</sup> All non-hydrogen atoms were refined anisotropically. Hydrogen atom positions were calculated and isotropically refined as riding models to their parent atoms. A summary of selected data collection and refinement parameters can be found from the Supporting Information (Table S1).

## Computational methodology

The calculation of zero-field splitting parameters (D and E) were carried out with two different software packages: MOLCAS<sup>25</sup> and ORCA.<sup>26</sup> We have used MOLCAS (along with the SINGLE\_ANISO<sup>27</sup> code) to carry out CASSCF calculations of the energy states of the Co<sup>II</sup>Y<sup>III</sup> complexes. Then, spin-orbit coupling has been

considered, as implemented in the SO-RASSI (Restricted Active Space State Interaction) approach, to mix up these energies and obtaining the final energy states. In these calculations we have employed an all electron ANO-RCC basis set:<sup>28</sup> Co atoms (6s5p4d2f), N (4s3p2d1f), C (3s2p) and H (2s). Similar CASSCF calculations were performed with ORCA. In this case, spin-orbit effects were included using the quasi-degenerate perturbation theory (QDPT)<sup>29</sup> and N-electron valence perturbation theory to second order (NEVPT2)<sup>30</sup>. Scalar relativistic effects were taken into account by second-order Douglas-Kroll-Hess (DKH) procedure.<sup>31</sup> In these calculations, all the atoms are described by the def2-TZVPP basis set,<sup>32</sup> including the corresponding auxiliary basis sets for correlation and Coulomb fitting. In both sets of calculations, the active space includes seven electrons in five 3d-orbitals of Co(II) CAS (7,5). We have included all 10 states for the  $2S+1 = 4$  (quartet) states arising from the 4F and 4P terms of Co(II), and all the 40 states for the respective  $2S+1 = 2$  (duplet) states arising from the 2P, 2D (twice), 2F, 2G and 2H terms of Co(II) ion.

Splitting of the d-orbital was obtained with a new *ab initio* ligand field theory that was recently developed. Eigenvalues and eigenfunctions from CASSCF/NEVPT2 calculations were used to reconstruct the matrix of the ligand field Hamiltonian, which was parameterized in terms of the 5x5 one-electron ligand field matrix elements accounting for the splitting of the nominal 3d-orbitals due to interaction with the ligand donor atoms, as well as the Racah parameters B and C to take inter-electronic repulsion into account. Since all matrix element of the ligand field Hamiltonian matrix are linearly depended on these parameters, the latter can be determined via a least squares fitting method to the corresponding *ab initio* values of the same matrix elements.<sup>33</sup> The results of these calculations are given in Table 2 and Table S2.

## Results and Discussion

We have recently shown that the heptadentate compartmental ligand  $H_2L = N,N',N''$ -trimethyl- $N,N''$ -bis(2-hydroxy-3-methoxy-5-methylbenzyl)diethylenetriamine (see Figure 1), which has an inner  $N_3O_2$  pocket and an outer  $O_2O_2$  coordination site that have preference for transition metal and lanthanide ions, respectively, is able to form a stable  $Co_{II}Y_{III}$  complex  $[Co(\mu-L)(\mu-OAc)Y(NO_3)_2]_{10}$  in which the metal ions are triply bridged by two phenoxide groups and one acetate anion. This latter ligand is required in order to saturate the octahedral coordination sphere of the  $Co_{II}$  ion. Now, using the same ligand, we have prepared three new dinuclear  $Co_{II}Y_{III}$  complexes, in which the ancillary bridging ligands between  $Co_{II}$  and  $Y_{III}$  ions are can be nitrate, benzoate and 9-anthracene carboxylate (9-AC).

The reaction of  $H_2L$  with  $Co(NO_3)_2 \cdot 6H_2O$  and subsequently with  $Y(NO_3)_3 \cdot 6H_2O$  in methanol in 1:1:1 molar ratio afforded the dinuclear complex  $[Co(\mu-L)(\mu-NO_3)Y(NO_3)_2]$  **1**. When benzoic acid and triethylamine are added to the resulting solution for the preparation of **1** in 1:1:1:1:1 molar ratio, the compound  $[Co(\mu-L)(\mu-Bz)Y(NO_3)_2]$  **2** was obtained. The same reaction but using 9-anthracene carboxylic acid instead of benzoic acid afforded the complex  $[Co(\mu-L)(\mu-9-AC)Y(NO_3)_2] \cdot 2CH_3OH \cdot 2H_2O$  **3** (Figure 1).

## X-Ray Structures

Selected bond lengths and angles for compounds **1-3** are given in Table 1, whereas their molecular structures are given in Figures 1. Compound **1** is isostructural to a Ni-Tb previously reported by us<sup>34</sup> and its structure consists of isolated dinuclear molecules in which the  $Co^{II}$  and  $Y^{III}$  are triply bridged by two phenoxide groups pertaining to the dideprotonated ligand ( $L^{2-}$ ) and one nitrate anion (Figure 1).

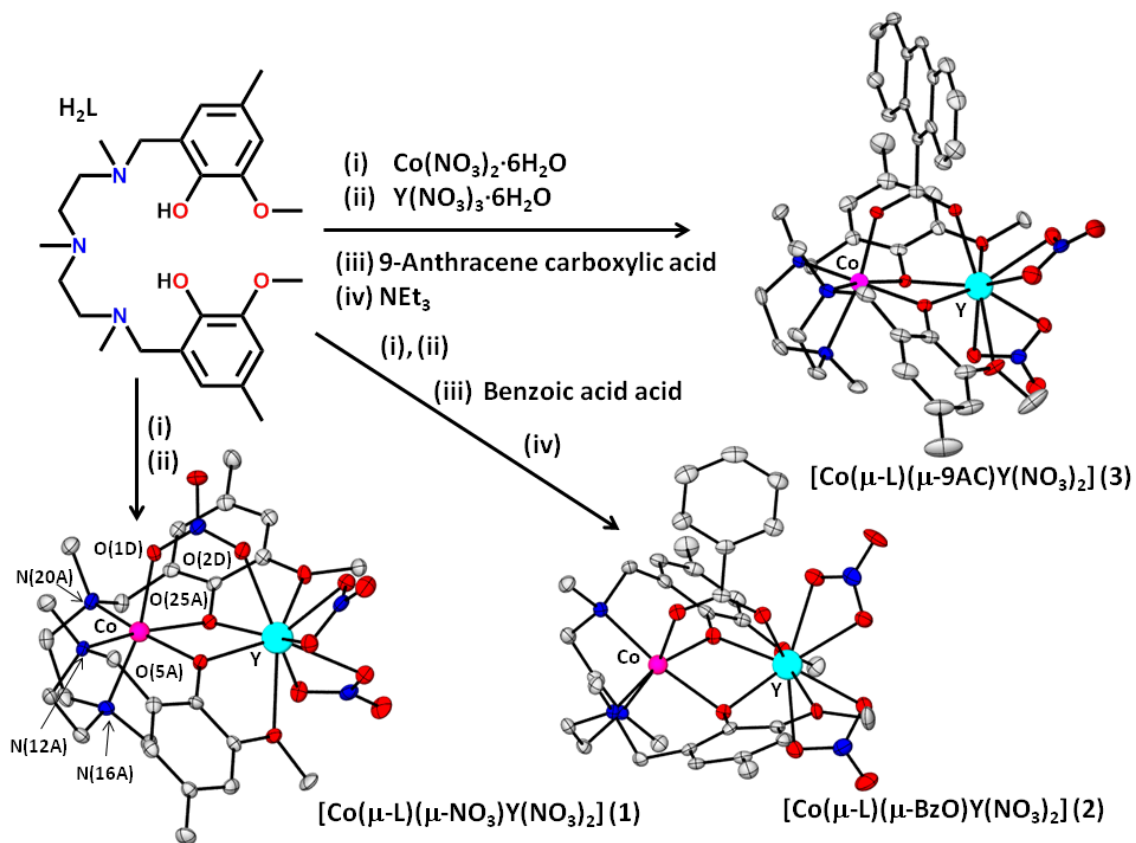


**Figure 1.** Synthesis and perspective view of the structures of compounds **1-3**. Colour code: N = blue, O = red, Co = pink, Y = light blue, C = grey. Hydrogen atoms are omitted for the sake of clarity.

As expected, the  $Co^{II}$  ion is located in the inner site of the ligand and shows a trigonally distorted coordination polyhedron, where the three amine nitrogen atoms and, therefore, the three oxygen atoms belonging to the phenoxide and nitrate bridging groups assume a *fac* configuration. The structures of **2** and **3** are very similar to that of **1** but replacing the nitrate bridging ligand by benzoate or 9-anthracene carboxylatoligands, respectively, adopting a syn-syn bridging coordination mode (Figure 1).

In all these complexes the  $Y^{III}$  atom exhibits a  $YO_9$  coordination sphere, which is always made of two bridging phenoxide and two methoxy oxygen atoms belonging

to the L<sub>2</sub>- ligand, whereas the remaining five oxygen atoms pertain to two bidentate nitrate ancillary ligands and to the nitrate, benzoate and 9-AC bridging ligands.

The bridging coordination of nitrate, benzoate and 9-AC ligands provokes the folding of the Co( $\mu$ -diphenoxido)Y bridging fragment with average O-Co-O-Y hinge angles of 15.16 °, 19.20 ° and 18.74 ° for **1-3**, respectively (the hinge angle is the dihedral angle between the O-Ni-O and O-Y-O planes in the bridging fragment), whereas the Co-Y distances are found to be 3.445 Å, 3.432 Å and 3.418 Å for **1-3**, respectively. In view of this, it is clear that the change of the ancillary bridging ligand between Co<sup>II</sup> and Y<sup>III</sup> (nitrate, benzoate and 9-AC) induces small but significant variations in the structural parameters of the [Co( $\mu$ -diphenoxido)Y] bridging region, which slightly modify the Co<sup>II</sup> coordination sphere (see Table 1). Thus, the distortion of the CoN<sub>3</sub>O<sub>3</sub> coordination polyhedron with regard to ideal six-vertex polyhedra, which was calculated by using continuous shape measure theory and SHAPE software (Table S3),<sup>35</sup> indicated that the Co<sup>II</sup> coordination polyhedron for these compounds is found in the OC<sub>6</sub>↔TPR<sub>6</sub> deformation pathway but much closer to the OC-6 geometry. The shape measure values for the OC-6 polyhedron are 2.057, 1.610 and 1.680 for complexes **1**, **2** and **3**, respectively, indicating the distortion follows the order **1**>**2** ≈**3**. The smaller the hinge angle, the larger is the distortion of the Co<sup>II</sup> coordination sphere from the OC-6 geometry.

### **Magnetic Properties**

The temperature dependence of the molar magnetic susceptibility ( $\chi_M$ ) per Co<sup>II</sup> ion of complexes **1-3** in the 2-300 K temperature range under an applied magnetic field of 1000 Oe are given in Figure 2 (the plot for complex **3** is given as an example) and Figures S1 and S2 in the form  $\chi_M T$  versus T. The  $\chi_M T$  values at room temperature for complexes **1-3** of 2.70, 2.06 and 3.29 cm<sup>3</sup>mol<sup>-1</sup>K, respectively, are greater than the

expected for a orbitally non-degenerate ground state  $S = 3/2$  spin of  $1.875 \text{ cm}^3\text{mol}^{-1}\text{K}$ , which is indicative of unquenched orbital contribution of the Co(II) ion in distorted octahedral geometry. When the temperature is lowered, the  $\chi_M T$  product decreases first slightly from room temperature to 70 K and then in a sharper manner to reach values of 1.65, 1.86 and 1.92  $\text{cm}^3\text{mol}^{-1}\text{K}$  at 2 K, for **1-3**, respectively. This decrease is mainly due to spin-orbit coupling (SOC) effects.

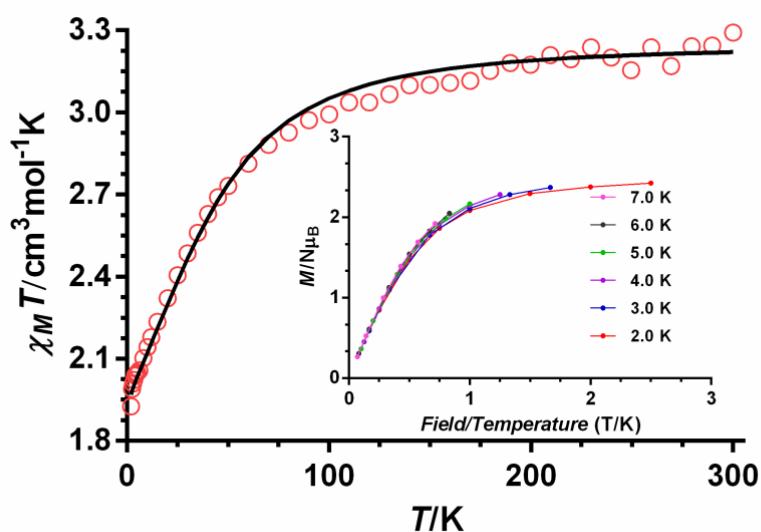


**Figure 2.-** Temperature dependence of  $\chi_M T$  for compound **3**. The solid line represents the best fit curve (see text).  $M$  vs  $H/T$  plot for compound **3** (inset).

If for the sake of ease, we consider a  $C_{3v}$  local symmetry for the distorted octahedral  $\text{CoN}_3\text{O}_3$  coordination polyhedron of **1-3**, the triplet  $4T_{1g}$  ground state for the ideal  $O_h$  symmetry splits into an orbital singlet  $4A_2$  and an orbital doublet  $4E$ , with an energy gap between them described by the axial splitting parameter,  $\Delta$ . The  $4A_2$  and  $4E$  levels are additionally split by second order spin-orbit coupling leading to two and four Kramers doublets, respectively. When  $\Delta$  is large enough and positive only the two lowest Kramers doublets coming from the  $4A_2$  ground term,  $\Gamma_6$  and  $\Gamma_7$ , are thermally populated and the energy gap between these two Kramers doublets can be considered as a zero-

field splitting (ZFS) within the quartet state. If so, the magnetic properties can be interpreted by using the following Hamiltonian:

$$H = D[S_z^2 - S(S + 1)/3] + E(S_x^2 - S_y^2) + g\mu_B HS,$$

where  $S$  is the spin ground state,  $D$  and  $E$  are the axial and transverse magnetic anisotropies, respectively,  $\mu_B$  is the Bohr magneton and  $H$  the applied magnetic field. If  $E = 0$ , then  $2D$  symbolize the energy gap between  $\pm 1/2$  and  $\pm 3/2$  Kramers doublets (KD) arising from second order SOC of the quartet ground state. If  $D > 0$  the  $M_s = \pm 1/2$  doublet lies below the  $M_s = \pm 3/2$  doublet on the energy scale and if  $D < 0$ , *vice versa*. The temperature dependence of the magnetic susceptibility data for **1-3** was fitted with the above Hamiltonian using the PHI program<sup>36</sup> (Figure 2 and Figures S1 and S2). The best fits of the data were obtained by fixing  $E = 0$  and using isotropic  $g$  tensors. The following magnetic parameters were extracted from the fits:  $D = +42.0$  cm<sup>-1</sup>,  $g = 2.41$  for **1**,  $D = +53.0$  cm<sup>-1</sup>,  $g = 2.57$  for **2** and  $D = +51.80$  cm<sup>-1</sup>,  $g = 2.63$  for **3**. Nevertheless, it should be noted that reasonably good fits can also be obtained when: (i)  $E$  are fixed to zero and axial tensors  $g_{\perp}$  and  $g_{\parallel}$  are used; (ii)  $D$  and  $E$  is allowed to freely vary using an isotropic  $g$  tensor; (iii) negative  $D$  values are employed. In these cases,  $|D|$  values are found in the ranges 40.0-42.1 cm<sup>-1</sup>, 50.0-54.1 cm<sup>-1</sup> and 49.1-54.1 cm<sup>-1</sup> for **1-3**, respectively. In view of these results, we can conclude that these compounds exhibit large  $|D|$  values, which are found in the 40-55 cm<sup>-1</sup> range. These values are close to that previously reported for the analogous complex [Co( $\mu$ -L)( $\mu$ -OAc)(NO<sub>3</sub>)<sub>2</sub>].<sup>10</sup> In view of the above results, the magnitude of the ZFS (the energy separation,  $\delta$ , between the  $m_s = \pm 1/2$  and  $m_s = \pm 3/2$  Kramers doublets), which is given by  $\delta = 2(D^2 + 3E^2)^{1/2}$ , should be for **1-3** in the range 80-120 cm<sup>-1</sup>. When the ZFS is very large, as in the case of

complexes **1-3**, the  $M$  vs  $H/T$  isotherms depend only slightly on temperature (see Figure 2 for compound **3** and Figures S1 and S2 for compound **1** and **2**) so that the ZFS parameters cannot be accurately obtained from the fitting of the temperature dependence of the magnetization at different magnetic fields to the above Hamiltonian.

In order to unambiguously know the sign of  $D$ , we have performed low-temperature (down to 5 K) high-frequency and -field EPR (HFEPR) measurements in the 50–650 GHz, and 0–14.5 Tesla range, respectively, on powder samples of **1-3** (Figure 3 and Figures S3 and S4). All the HFEPR spectra are characteristic for high-spin ( $S = 3/2$ )  $\text{Co}^{\text{II}}$  with large positive axial ZFS parameter  $D$ . No transitions between the  $m_s = \pm 1/2$  and  $\pm 3/2$  KDs were observed because the energy gap  $\delta$  between these doublets is significantly larger than the highest available energy of the sub-THz wave quantum (23  $\text{cm}^{-1}$ ). However, the observed resonances could be unequivocally attributed to a transition within the  $m_s = \pm 1/2$  manifold (this transition is allowed because  $\Delta m_s = \pm 1$ ), thus confirming that the  $m_s = \pm 1/2$  KD lies lower on the energy scale than the  $m_s = \pm 3/2$  KD and therefore  $D$  is positive (Figure 3). Although the magnitude of the ZFS cannot be extracted from the transition within the  $m_s = \pm 1/2$  manifold, however, it allows to evaluate the E/D rhombicity factor. This factor is found to be between the limits  $0.059 < E/D < 0.225$  for complexes **1-3**, probably close to the upper limit (see Table S4). In the case of  $D < 0$ , the lower-lying KD is  $m_s = \pm 3/2$ ; the transition within this manifold is nominally forbidden ( $\Delta m_s = \pm 3$ ) and the EPR spectrum is usually absent if  $E/D \sim 0$ .

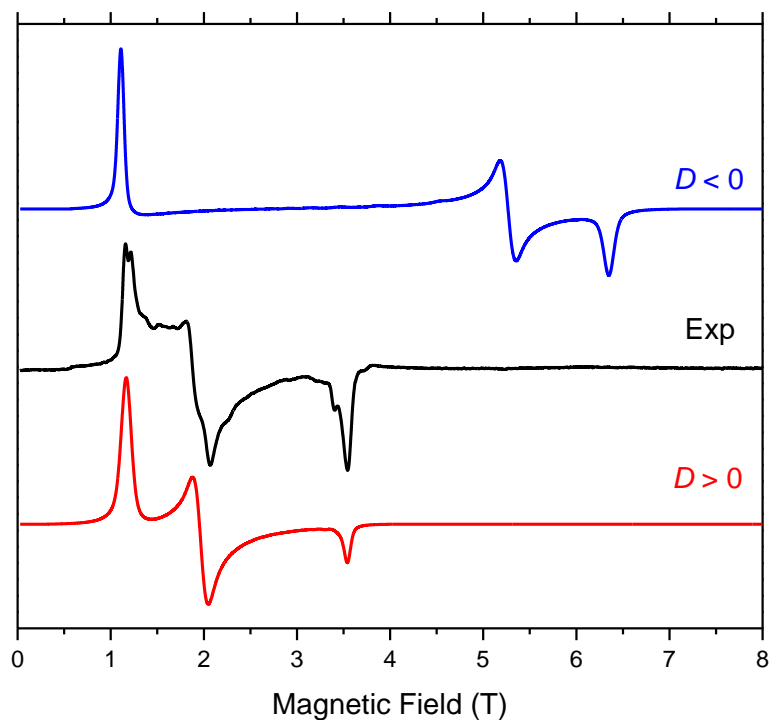


**Figure 3.** A 101.6 GHz spectrum of **3** at 10 K (black trace) accompanied by two simulations using the following parameters:  $|E/D| = 0.174$ ,  $g_{\perp} = 2.53$ ,  $g_{\parallel} = 2.24$ . Red trace:  $D > 0$ ; blue trace:  $D < 0$ . In each case  $|D/|$  was fixed at  $56.4 \text{ cm}^{-1}$  (the value obtained by NEVPT2 calculations) and the rhombicity of the zfs tensor was calculated under assumption of an axial g-tensor (i.e. ignoring the rhombicity of g-tensor).

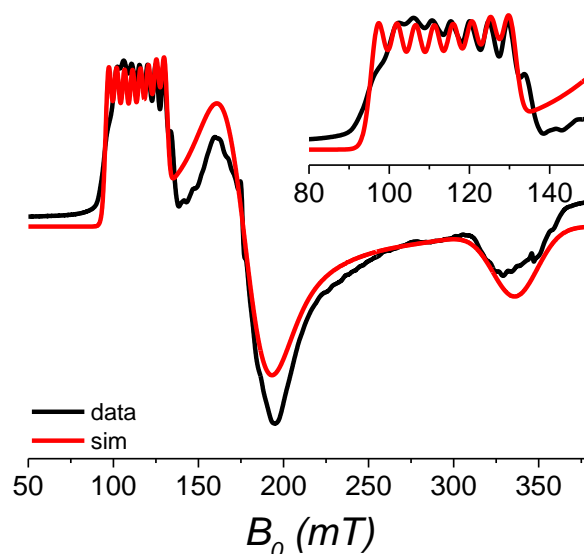


**Figure 4.-** X-band EPR spectrum of a diluted sample of **3''** (Co/Zn= 1/20). Experimental and simulated spectrum (with the effective spin  $S'=1/2$  and  $g'_x = 6.1(3)$ ,  $g'_y = 3.9(1)$ ,  $g'_z = 2.05(5)$ , and  $A'_x = 380(30)$  MHz) are shown in black and red colours, respectively.

X-Band EPR spectra of **3''** (magnetically diluted version of **3** with a Co<sub>II</sub>/Zn<sub>II</sub> ratio = 1/20, see Figure 4) reveal three EPR lines at 115, 180, and 340 mT (the EPR spectrum of **3** was quite complex, probably due to intermolecular interactions). All three lines decrease in intensity with increasing temperature (see Figure S5). The low-field line was observed to be splitted in 8 partly overlapping lines, most probably due to hyperfine interaction with the <sup>59</sup>Co nucleus with  $I = 7/2$ . Simulations with an effective spin  $S' = 1/2$  (assuming that only transitions between the ground state KD are observed) were successful with:  $g'_x = 6.1(3)$ ,  $g'_y = 3.9(1)$ ,  $g'_z = 2.05(5)$ , and  $A'_x = 380(30)$  MHz.

In order to accurately determine the magnitude of the ZFS we used FD-FT THz-EPR spectroscopy. This technique allows to directly extracting the value of the ZFS, i.e the energy separation  $\delta$ . However, no information whatsoever on the signs of the ZFS parameters can be obtained. FD-FT THz-EPR records the transition between the two

KDs, regardless of which of the doublets is lower in energy. Because of the limited access to the FD-FT THz-EPR technique, we have only recorded the spectrum of **3** (Figure 5).

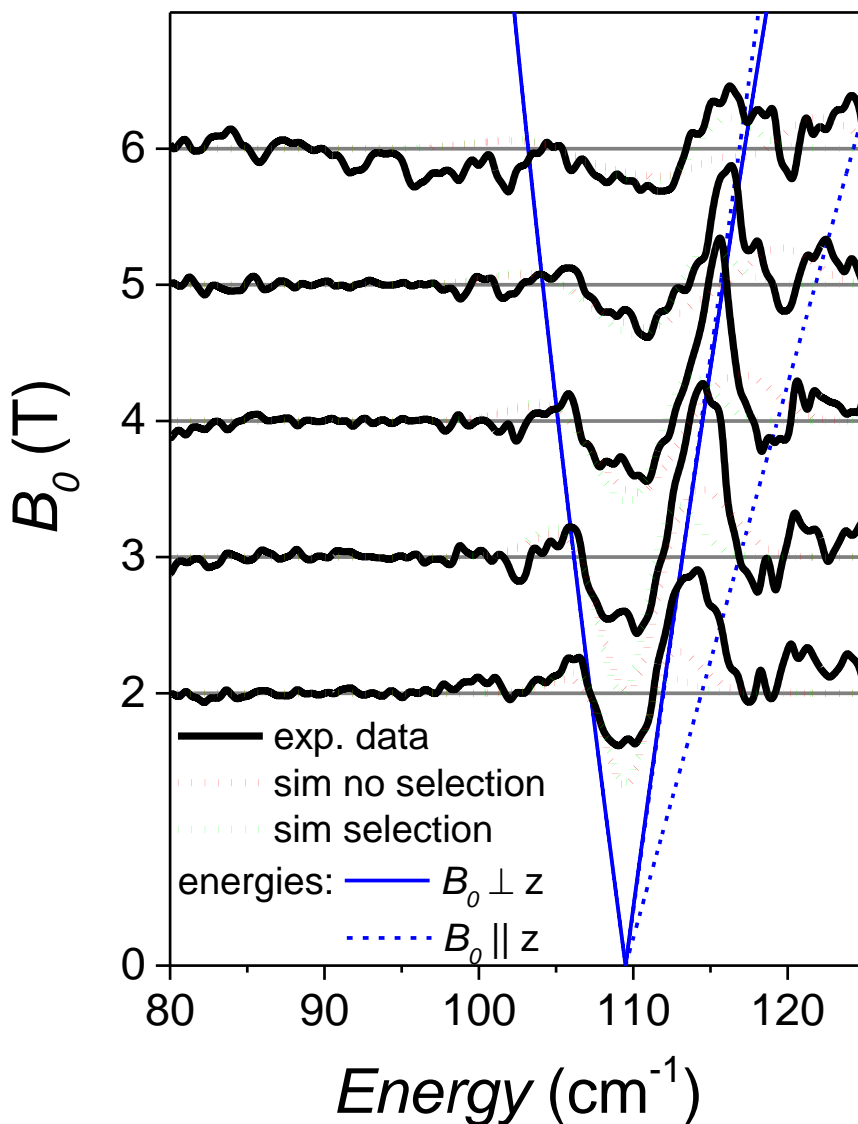


**Figure 5:** FD-FT THz-EPR MDS spectra of compound **3**. Experimental results are shown as black solid lines. Spectra are offset according to the external magnetic field at which they were measured. Simulations with  $D = 56.6(4) \text{ cm}^{-1}$ ,  $E = 8.5(6) \text{ cm}^{-1}$  ( $\frac{E}{D} = 0.15(1)$ ),  $g_{\perp} = 2.5(1)$ , and  $g_{\parallel} = 2.18(5)$  are included as dotted lines. In red a simulation considering all transitions is shown. A simulation, which excludes the transition from

the ground state to the highest excited state, is shown in green. The transition energy for transitions originating from the ground state are shown for external magnetic field applied along the three principal axes of the compounds as blue lines (dotted:  $B_0 \parallel x$  and solid:  $B_0 \parallel z$ , for).

A minimum could be observed in the MDS at  $B_0 = 2$  T, corresponding to absorption in the absence of a magnetic field at an energy of  $109.5 \text{ cm}^{-1}$ . This feature split both to higher and lower energies with increasing magnetic field and, consequently, assigned to be of magnetic origin. On both the low- and high-energy sides of the minimum at  $109.5 \text{ cm}^{-1}$ , maxima were observed, where the latter was observed much more pronounced. With increasing magnetic field the minimum shift slightly towards higher energies and was observed as significantly broader. The direct measure of ZFS is in general an outstanding result, but especially for energies as high as  $109.5 \text{ cm}^{-1}$  or  $3.3 \text{ THz}$ . The value of  $\delta = 54.7(5) \text{ cm}^{-1}$  (extracted from FD-FT THz-EPR) can be converted into  $D$  using the  $E/D$  ratio of  $0.17$  obtained from HFEPR, which thus yields  $|D| = 52.5 \text{ cm}^{-1}$ . The same value made it possible to reproduce not only the HFEPR spectra of the bulk sample of **3**, but also the X-Band EPR spectrum of a  $5/100$  (Co/Zn) diluted complex **3''** at  $5 \text{ K}$  (the X-band spectrum of a bulk sample of **3**, which is shown in Figure 5, was quite complex. Probably this is due to inter-molecular exchange interactions, which are known to influence the spectrum of  $\text{CoII}$  complexes) with the following parameters,  $E/D = 0.15(1)$ ,  $g_{\perp} = 2.5(1)$ , and  $g_{\parallel} = 2.18(5)$ . Effective  $g'_i$  for the doublet ground state (modelled by an effective spin  $S' = 1/2$ ) are obtained from Pilbrow's equations as  $g'_x = 3.88$ ,  $g'_y = 6.07$ ,  $g'_z = 2.04$ . They agree within uncertainty with those obtained above.

Simulations of  $M$  vs  $H$  curves at different temperatures with  $D = 56.6(4)$   $\text{cm}^{-1}$ ,  $E = 8.5(6)$   $\text{cm}^{-1}$  ( $E/D = 0.15(1)$ ),  $g_{\perp} = 2.65$ , and  $g_{\parallel} = 2.2$  allow excellent agreement with measured  $\chi T$  and magnetization (see Figure S6). FD-FT THz-EPR spectra simulated with these parameters (Figure 5) were observed to reproduce the experimental results measured in the absence of a magnetic field. However, with increasing magnetic field the simulated feature (best observable for the maximum) shift faster to higher energy values than observed in the experimental spectrum. However, neglecting the transition from the ground state to the highest excited state the experimental results can be well reproduced (see Figure 5).

Compound **3** differs only by the ancillary bridging ligand from the analogous compound  $[\text{Co}(\mu\text{-L})(\mu\text{-OAc})\text{Y}(\text{NO}_3)_2](9\text{-AC})$  instead of acetato).<sup>10</sup> FD-FT THz-EPR measurements on this compound reveal that this subtle tuning on the  $\text{CoII}$  coordination sphere allows to increase the ZFS by roughly 10 %.<sup>37</sup>

In order to support the sign and magnitude of  $\delta$  for complexes **1-3**, we have performed electronic structure CASSCF calculations of the ZFS parameters  $D$  and  $E$  on the X-ray structures using either MOLCAS<sup>25</sup> or ORCA<sup>26</sup> and software packages. Likewise, NEVPT2 calculations were carried out with ORCA. The SO-RASSI approach included in MOLCAS and quasi-degenerate perturbation theory (QDPT) implemented in ORCA produce very similar results, which indicate that the computed  $D$  values (Table 2) for the three complexes are overestimated with regard to those obtained experimentally from magnetic data and FD-FT THz-EPR spectra. However, the computed  $D$  values with NEVPT2 RASSI calculations are smaller and closer to the experimental values. Interestingly, the  $\delta$  value for **3** of  $120.2$   $\text{cm}^{-1}$  agrees rather well with that extracted from FD-FT THz-EPR spectroscopy of  $109.5$   $\text{cm}^{-1}$ . The difference between experimental and calculated  $D$  values are most likely due, among other

reasons, to limitations inherent to the theoretical methods, certain inaccuracy of the magnetic data, and the possible slight changes of the Co<sub>II</sub> coordination sphere at low temperature with regard to the crystal structures employed in the theoretical calculations.

Calculations support  $D > 0$  values for the three complexes and confirm that  $D$  values follow the same order as in the experimental results:  $D_1 < D_2 \sim D_3$ . Finally, it should be pointed out that the computed  $|E/D|$  values agree rather well with those extracted from HFEPR spectra (see Table S4).

**Table 2.-** CASSCF + RASSI and NEVPT2 + RASSI values of  $D$  and  $|E|$  and first excitation energies calculated at the spin-free CASSCF and NEVPT2 levels ( $\Delta E_{1c}$ ), respectively, and after the inclusion of spin-orbit effects ( $\delta E_{1c}$ )

Compound	$D_{\text{cal}} / \text{cm}^{-1}$	$ E/D _{\text{calc}}$	$ E/D _{\text{HFEPR}}$	$\Delta E_{1c} / \text{cm}^{-1}$	$\delta E_{1c} / \text{cm}^{-1}$
<b>1</b>	64.7 <sub>a</sub> /65.7 <sub>b</sub> /49.7 <sub>c</sub>	0.05 <sub>a</sub> /0.06 <sub>b</sub> /0.07 <sub>c</sub>	0.09	873	100.1
<b>2</b>	77.6/78.8/60.9	0.14/0.16/0.18	0.22	807	127.7
<b>3</b>	72.7/74.3/56.4	0.16/0.17/0.21	0.18	890	120.2

<sup>a</sup> and <sup>b</sup> CASSCF+RASSI with MOLCAS and ORCA, respectively. <sup>c</sup>NEVPT2 + RASSI with ORCA

It has been recently shown from theoretical calculations<sup>11a</sup> that positive values for  $D$  are expected for Co<sub>II</sub> octahedral complexes, whereas  $D < 0$  values are predicted for trigonal prismatic Co<sub>II</sub> complexes. This prediction is based on the evaluation of  $D_{ii}$  components ( $i = x, y, z$ ), which determine the sign and magnitude of  $D$ . These components depend inversely on the energy of the  $d$ -orbitals, specifically on the excitation energies, as well as of the  $m_l$  values of the orbitals involved in the lowest energy transitions. Therefore, there exists a correlation between the computed  $D$  values and the energy of the quartets states before applying spin-orbit coupling. The distortion

of the octahedral geometry in these compounds gives rise to a distribution of  $d$ -orbitals in which the  $t_{2g}$  orbitals in Oh are not degenerate and very close in energy (see figure S7). The same can be ascribed for the  $d$  orbital arising from the  $e_g$  Oh orbitals after distortion. In this situation, the first two excited quartet states (which arise for the interchange of one electron between the double-occupied  $d$  orbitals and the semi-occupied orbital coming from  $t_{2g}$  orbitals in Oh) and the ground quartet state (GQS) are close in energy (see Table S2). For example, in the case of **3**, these two quartet states are located 890  $\text{cm}^{-1}$  and 1479  $\text{cm}^{-1}$  above GQS. Therefore, a strong contribution from these two first excited states to  $D$  is expected, being the contribution of the first excited state larger than that of the second excited state. The other excited quartet states are much higher energies above the GQS and consequently their contribution to  $D$  is expected to be very weak. If  $dxz$  and  $dyz$  orbitals are double-occupied and the  $dxy$  orbital is semi-occupied, the orbitals involved in the first excitations are related by changes of  $\pm 1$  in  $m_l$  and therefore  $D$  should be positive, which is in good agreement with the above indicated HFEPR results and theoretical calculations for complexes **1-3**. This prediction fully agrees with the results from CASSCF + RASSI and NEVPT2 + RASSI calculations with ORCA given on Table 3 and Table S2.

Table 3.-Contributions to  $D$ -tensor from NEVPT2 + RASSI calculations

Compound	<b>1</b>		<b>2</b>		<b>3</b>	
	$D$	$E$	$D$	$E$	$D$	$E$
$4\Phi_1$	27.486	0.371	35.698	34.336	34.601	33.883
$4\Phi_2$	24.279	1.619	23.644	-21.829	22.217	-21.343
$4\Phi_3$	0.690	1.316	-0.296	-1.003	-0.885	0.026
$4\Phi_4$	0.947	0.614	-2.153	-0.466	-1.358	-0.045
$4\Phi_5$	-9.622	-0.271	-5.104	0.921	-7.349	0.321

It is worth noting that there is a non-linear correlation between the calculated  $D$  values for **1-3** and the analogous  $[\text{Co}(\mu\text{-L})(\mu\text{-OAc})(\text{NO}_3)_2]$ ,<sup>10</sup> and the distortion from the octahedral geometry quantified by the shape measures parameter ( $S$ ): the larger the distortion (larger  $S$ ) the smaller is the  $D$  value (see Figure S8). The results for this family of complexes, that only differ in the ancillary bridging ligand, clearly show how this slight modification of the  $\text{Co}_{\text{II}}$  coordination sphere significantly affects the magnitude of ZFS. This exemplifies that the ZFS is an extremely sensitive probe for the electronic structure. Hence, the whole molecular structure has to be considered in targeted synthesis with the aim to reach high ZFS.

Dynamic alternating current (*ac*) magnetic susceptibility measurements were carried out for complexes **1-3** at a 3.5 Oe *ac* field. None of these complexes showed out-of-phase signals ( $\chi''_{\text{M}}$ ) under a zero *dc* applied field, thus pointing out that either these complexes do not exhibit SIM behavior below 2 K or the magnetization relaxation takes place through a ground state fast quantum tunneling process (QTM), which can be induced by intermolecular and/or strong hyperfine interactions with the  $I = 7/2$  nuclear spin of the cobalt (II) ion. For Kramers ions, like  $\text{Co}_{\text{II}}$ , the direct and QTM relaxation processes in a given doublet state are forbidden in strictly zero field.<sup>9</sup> However, nuclear-spin interactions, as well as a transversal magnetic field created by intermolecular interactions (which is proportional to the matrix element of the transversal magnetic moments between the two doublet states) split the doublet states providing relaxation channels for direct and QTM processes. After applying a 1000 Oe *dc* field to partly or fully eliminate the QTM fast relaxation, only complex **1** showed a clear frequency dependency of the in-phase ( $\chi'_{\text{M}}$ ) and out-of-phase signals ( $\chi''_{\text{M}}$ ) with maxima in the 3K (200 Hz) - 5.5 K (1488 Hz), as it can be observed in Figure 6 and Figures S9-S10.

Application of a magnetic field of 1000 Oe was also shown to be required to observe slow relaxation of magnetization in the analogous complex  $[\text{Co}(\mu\text{-L})(\mu\text{-OAc})(\text{NO}_3)_2]$ .<sup>10</sup> The presence of field is necessary because, as it has been recently shown for Kramers ions (particularly for those with  $D > 0$ ), at zero *dc* field the electronuclear spin states arising from the hyperfine interactions have, if any, negligible magnetic moments and so slow relaxation cannot be observed.<sup>9</sup> However, when a *dc* magnetic field is applied, the electronuclear spin states attain a non-zero magnetic moment and slow relaxation is observed. It is worth mentioning that the magnetic diluted compounds **2'** and **3'** (see below), where intermolecular interactions are suppressed, present, in contrast to the undiluted complexes **2** and **3**, field induced SIMs behaviour. Therefore, the absence of slow relaxation of **2** and **3** under a *dc* applied field of 1000 Oe could be due to the existence of larger intermolecular interactions than in complexes **1** and  $[\text{Co}(\mu\text{-L})(\mu\text{-OAc})(\text{NO}_3)_2]$ . In order to support this assumption, we have analyzed the intermolecular interactions in compounds **1-3**. These interactions can arise from spin-spin dipolar interactions, which vary approximately with the  $(\mu^2/r^3)$  ratio, where  $\mu$  is the magnetic moment of the magnetic dipole and  $r$  is the nearest neighbour distance between magnetic dipoles. In this regard, the shortest Co...Co intermolecular distance for **2** of 8.423 is larger than that observed for **1** but, at variance with this compound, **2** exhibits weak  $\pi$ - $\pi$  stacking interactions involving phenyl rings of the compartmental ligand with a distance between the ring centroids of 3.60 Å (Figure S11). In complex **3**, the shortest Co...Co intermolecular distance of 7.469 Å is shorter than those found for **1** and  $[\text{Co}(\mu\text{-L})(\mu\text{-OAc})(\text{NO}_3)_2]$ <sup>10</sup> and there exist  $\pi$ - $\pi$  stacking interactions between the anthracene rings with distances between the aromatic carbon atoms of parallel anthracene rings shorter than 3.3 Å (Figure S12). Therefore, in **3** the intermolecular interactions are clearly stronger than in **1** and  $[\text{Co}(\mu\text{-L})(\mu\text{-OAc})(\text{NO}_3)_2]$ <sup>10</sup>, whereas in **2** the situation is

less clear. However, if we consider the atoms in the virtual line connecting nearest neighbours  $\text{Co}_{2+}$  ions (with the shortest  $\text{Co}\cdots\text{Co}$  distance), which can protect  $\text{Co}_{2+}$  ions from the dipolar influence of nearest neighbouring  $\text{Co}_{2+}$  metal ions, the existence of strong intermolecular interactions in **2** and **3** is clearly supported (Figure S13). In the case of **1** and  $[\text{Co}(\mu\text{-L})(\mu\text{-OAc})(\text{NO}_3)_2]_{10}$ , the carbon atoms of the triamine chelate rings of the  $\text{L}_2$ - ligand shield the  $\text{Co}_{2+}$  from the direct influence of the nearest neighbouring  $\text{Co}_{2+}$  atoms, thus precluding strong dipolar interactions. In **2** and **3**, however, the  $\text{Co}_{2+}$  are not directly shielded and dipolar interactions are larger than in **1** and  $[\text{Co}(\mu\text{-L})(\mu\text{-OAc})(\text{NO}_3)_2]_{10}$ . In view of the above considerations it is reasonable to assume that the existence/absence of large intermolecular interactions seems to switch off/on the field induced SIM behaviour in this family of complexes. Nevertheless, this suggestion should be taken with caution as other factors such as the molecular arrangement in the crystal lattice, the crystal density, the speed of the sound in the solid and the strength of the spin-phonon interactions can influence QTM and spin-lattice direct and Raman relaxation process.

The relaxation times ( $\tau$ ) for **1** were determined from the fit of the frequency dependence of  $\chi''_{\text{M}}$  at each temperature to the generalized Debye model (Figures S10). The high temperature linear portion of the data were fitted to the Arrhenius expression ( $\tau^{-1} = \tau_0^{-1} e^{-U_{\text{eff}}/k_{\text{B}}T}$ ) for a thermally activated process (Orbach process) leading to an effective energy barrier for the magnetization reversal ( $U_{\text{eff}}$ ) of 23.9(8) K and a  $\tau_0$  value of  $1.5 \cdot 10^{-6}$  s. The Arrhenius plot built from the temperatures and frequencies of the maxima observed for the  $\chi''_{\text{M}}$  afforded similar  $U_{\text{eff}}$  and  $\tau_0$  values, as expected. It should be noted that the value of the effective energy barrier ( $U_{\text{eff}}$ ) is much lower than  $\delta$ , the energy gap between the ground and first excited doublet states, determined from temperature susceptibility data and from *ab initio* calculations (84 and 99.4  $\text{cm}^{-1}$ ,

respectively). Bearing in mind that the Orbach process takes place between real magnetic energy levels and complex **1** does not have energy levels below  $\sim 84 \text{ cm}^{-1}$ , the relaxation cannot proceed via an Orbach process with an  $U_{\text{eff}} = 23.9(8) \text{ K}$ . The field dependence of  $\tau^{-1}$  is given in Figure S and shows that  $\tau^{-1}$  decreases as the field increases, which indicates the progressive quenching of QTM. The  $\tau^{-1}$  vs  $H$  data were fitted to the following equation:  $\tau^{-1} = AH^4T + \frac{B_1}{1+B_2H^2} + C$  (equation 1), where the first two terms correspond to the direct and QTM relaxation processes, respectively, whereas the constant term  $C$  accounts for field independent relaxation processes (Figure S14). Then, the temperature dependence of  $\tau^{-1}$  for **1** was fitted to the equation  $\tau^{-1} = AH^4T + \frac{B_1}{1+B_2H^2} + BT^n$ , (equation 2), which takes into account the concomitant presence of direct, QTM and Raman relaxation processes (Figure S15). In order to avoid overparametrization, the parameters corresponding to QTM ( $B_1$  and  $B_2$ ) were fixed to those previously extracted (see above) from the field dependence of  $\tau^{-1}$ . The fits show (Figure S15) the dominance the Raman process above approximately 3 K, whereas below this temperature the direct is the main relaxation process. Although  $n = 9$  for Kramers ions,<sup>38</sup> however, depending on the structure of the levels and if optical phonons are considered,  $n$  values between 1 and 6 can be considered as acceptable.<sup>39</sup> The best fit of the experimental data (Figure 6 and Figure S15) afford the parameters indicated on Table 4. It should be noted that similar  $n$  values were obtained for compound  $[\text{Co}(\mu\text{-L})(\mu\text{-OAc})(\text{NO}_3)_2] \cdot 10,11\text{d}$

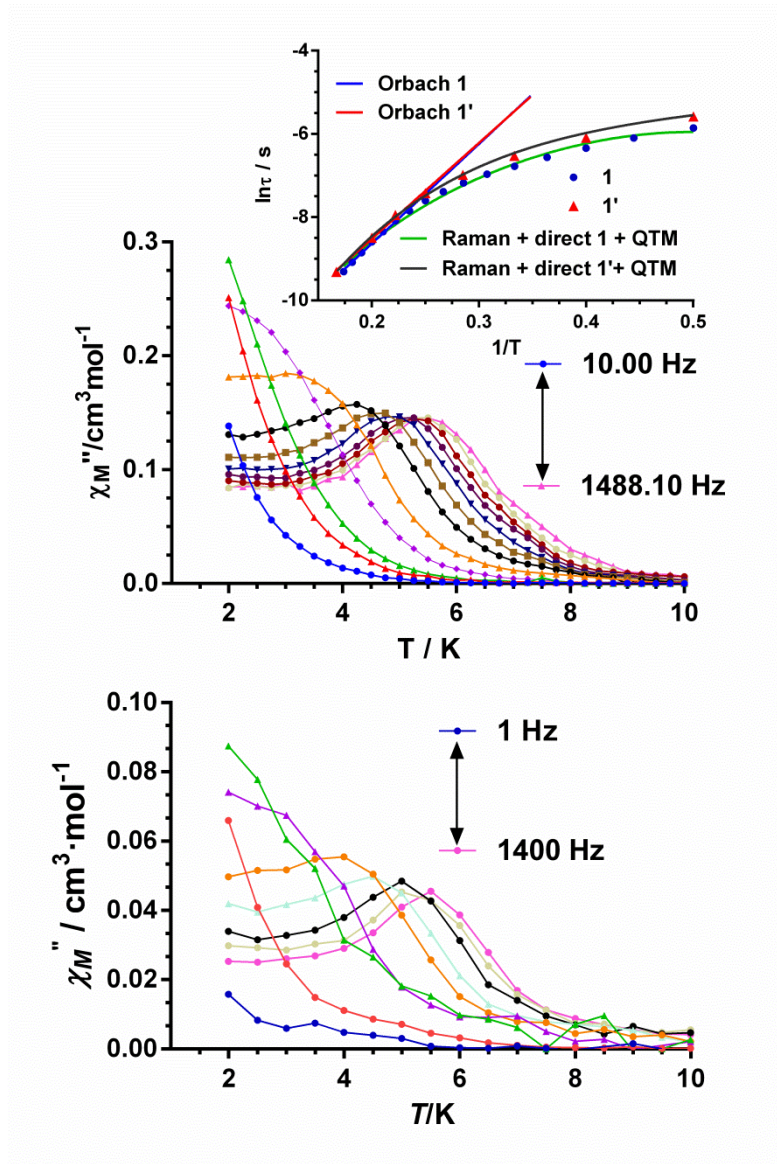


**Figure 6.** Temperature dependence of the out-of-phase components of the ac susceptibility at different frequencies for complexes **1**(middle) and **1'** (Co/Y 1:10) measured under 1000 Oe applied dc field. Solid lines are only guides for the eyes. Arrhenius plots (top inset). The blue and red lines correspond to **1** and **1'**, respectively. The green line represents the best fit to direct plus Raman relaxation processes.

The Cole-Cole plots for **1** show, in the temperature range 3.0-5.5 K, semicircular shapes that can be fitted by using the generalized Debye model (Figure S16). This fit afford a value for the parameter  $\alpha$ , which is related to the width of the distribution of

relaxation times, that is,  $\alpha = 1$  corresponds to an infinitely wide distribution of relaxation times, whereas  $\alpha = 0$  describes a single relaxation process. The extracted  $\alpha$  parameters are found in the 0.14 (3 K) - 0.05 (5.5 K) range, which would be compatible with the existence of more than one relaxation process in this temperature region. However, between 4 K and 5.5 K the  $\alpha$  values are found in the range 0.065-0.050, respectively, pointing out the existence of only one relaxation process. Thus, below approximately 4 K, Raman and direct processes are predominant and coexist, whereas above this temperature mainly takes place the Raman process.

**Table 4.-** Fitting Parameters for Orbach and Raman plus direct processes for compounds **1**, **1'**, **2'** and **3'**.

Complex	Orbach		Direct + Raman + QTM		
	$U_{\text{eff}}$ (K)	$\tau_0$ (s)	$A(s^{-1}K^{-1})$	$B(s^{-1}K^n)$	$n$
<b>1</b>	23.9(8)	$1.5 \cdot 10^{-6}$	159(10)	0.5(1)	5.7(1)
<b>1'</b>	24.8(1)	$1.4 \cdot 10^{-6}$	83(18)	1.2(4)	5.0(2)
<b>2'</b>	33.2(4)	$2.5 \cdot 10^{-7}$	60(1)	0.68(5)	5.57(5)
<b>3'</b>	34.6(9)	$2.3 \cdot 10^{-7}$	52(8)	0.05(7)	6.93(6)

Although suitable crystals for X-ray crystallography could not be obtained for complexes **1'**, however its X-ray powder diffractograms (Figure S17) clearly evidence that it has the same structure as the undiluted counterpart **1**. The diluted complex **1'** does not show significant changes in the positions of the maxima in the  $\chi''_{\text{MVS}}$ . T plot with

regard to the undiluted complex **1** (Figure 6 and Figures S18-S20). This fact is not unexpected in view of the almost negligible intermolecular interactions present in **1**. As in **1**, some QTM seems to remain in **1'**, which is evidenced by the fact that  $\chi''_M$  does not go to zero after the maxima (Figure 6). This behavior could be due to hyperfine interactions, which matches well with the fact that slow relaxation is only observed in the presence of applied magnetic field. As expected, the  $U_{\text{eff}}$  and  $\tau_0$  values for **1'** (see Table 4) are almost identical to those observed for **1**. As expected, compound **1'** presents similar field and temperature dependences of  $\tau^{-1}$  to those of observed **1** (Figure S14 right). The same treatment as for **1** of the  $\tau^{-1}$  vs  $H$  and  $\tau^{-1}$  vs  $T$  data led to the parameters indicated on Table 4. As in the case of **1**, the Raman process is dominant above approximately 3 K (Figure S15 right).

If the absence of maxima above 2 K in the  $\chi''_M$  vs.  $T$  plots of **2** and **3** were due, as indicated above, to fast QTM promoted by intermolecular interactions, the magnetic diluted counterparts of **2** and **3** could suppress these interactions and consequently to active SIM behavior. Taking this into consideration, we have prepared the diluted versions of complexes **2** and **3**. The structure of **2'** could be solved by X-ray single-crystal crystallography and the results indicate that this compound possesses the same structure as **2** with a Zn/Co = 1/11 molar ratio (XRPD of the bulk samples also supports the same structure for **2** and **2'**; Figure S21). Although suitable crystals for X-ray crystallography could not be obtained for complex **3'**, however its X-ray powder diffractogram clearly supports that this compound has the same structure as for the undiluted counterpart **3** (Figure S22).

In contrast to complexes **2** and **3**, their diluted counterparts **2'** and **3'** present slow relaxation of the magnetization under an applied field of 1000 Oe, with maxima in the  $\chi''_M$  vs  $T$  plot in the ranges 3.4 K (200 Hz)-7.4 K (10000 Hz) and 2.5 K (50 Hz)-5.5

K (1400 Hz), respectively (Figures 7 and Figure 8 and Figures S23-S26). Therefore, it is reasonable to conclude that the suppression of the intermolecular interactions by magnetic dilution activates the SIM behavior in these complexes. It is worth noting that several recent experimental studies have highlighted the important role played by intermolecular interactions in the magnetization relaxation process of transition metal based SIMs.<sup>40</sup> Nevertheless, as far as we know, **2** and **3** represent the first examples of transition metal complexes that do not present slow relaxation of the magnetization in the presence of applied magnetic field and, however, exhibit field induced slow relaxation of the magnetization by a further magnetic dilution. It should be noted magnetic dilution alone without applying magnetic field does not trigger the slow relaxation process.

The fit of the ac susceptibility data for **2'** and **3'** to the Debye model allowed for the extraction of  $\tau$  values at different temperatures (Figure S23 and S25, respectively), which were used to construct the Arrhenius plots (Figure 7 and Figure 8, inset). From the high temperature linear region of these plots, the following relaxation parameters were obtained  $U_{\text{eff}} = 33.2(4)$  K and a  $\tau_0$  value of  $2.5 \cdot 10^{-7}$  s for **2'** and  $U_{\text{eff}} = 34.6(9)$  K and a  $\tau_0$  value of  $2.3 \cdot 10^{-7}$  s. for **3'**. As for **1**, the extracted  $U_{\text{eff}}$  values for these compounds are also much lower than  $\delta$  values calculated from *ab initio* methods and extracted from magnetic measurements. Therefore, the relaxation cannot take place via a thermally activated Orbach process but via direct and Raman processes. In view of this, the temperature dependence of  $\tau^{-1}$  for **2'** and **3'** were fitted with equation 2 (inset figures 7 and 8, respectively) using the parameters extracted from the fit of the field dependence of  $\tau^{-1}$  to equation 1 (See Figures S27 and S28, respectively), affording the parameters gathered on Table 4. As for **1**, the fits show (Figure S29 and S30, respectively) the

dominance the Raman process above approximately 3 K, whereas below this temperature the QTM is the main relaxation process for  $3'$ .

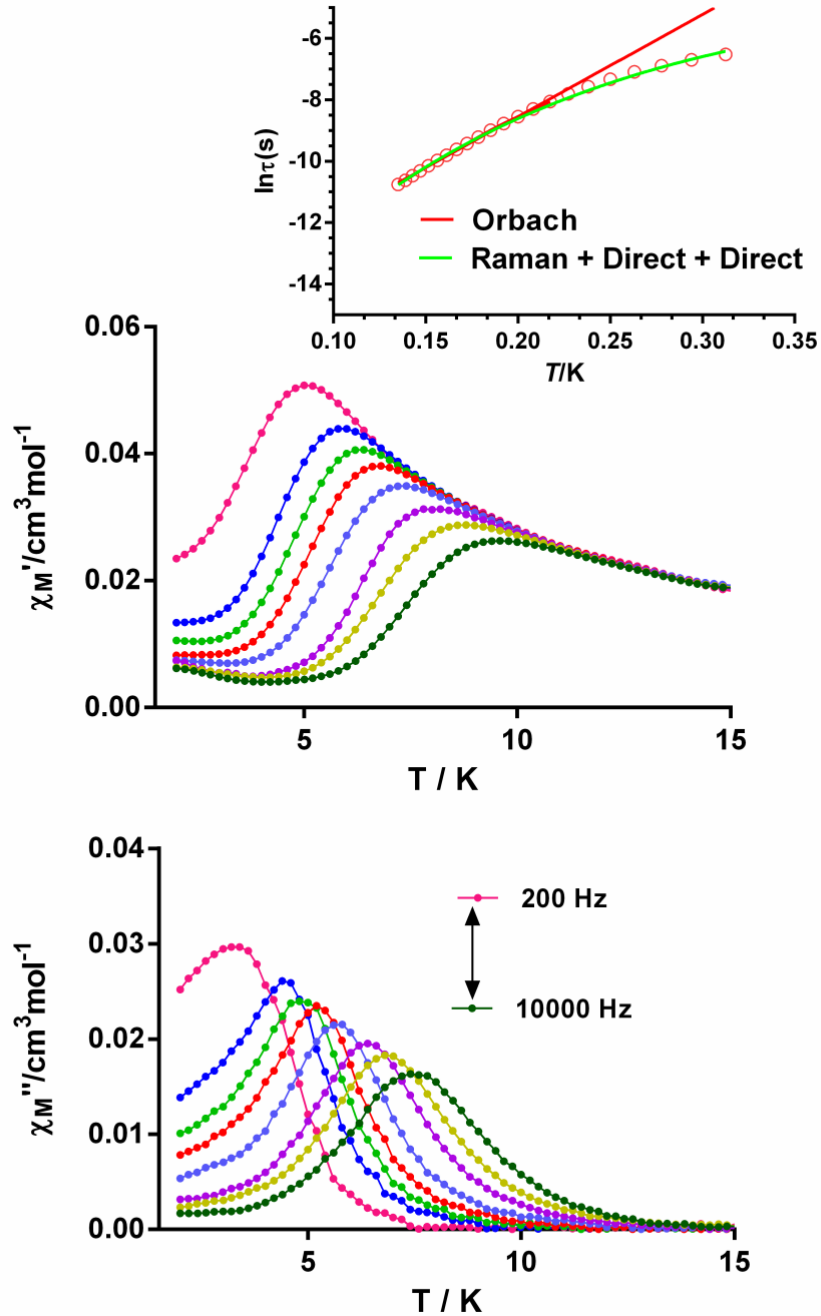
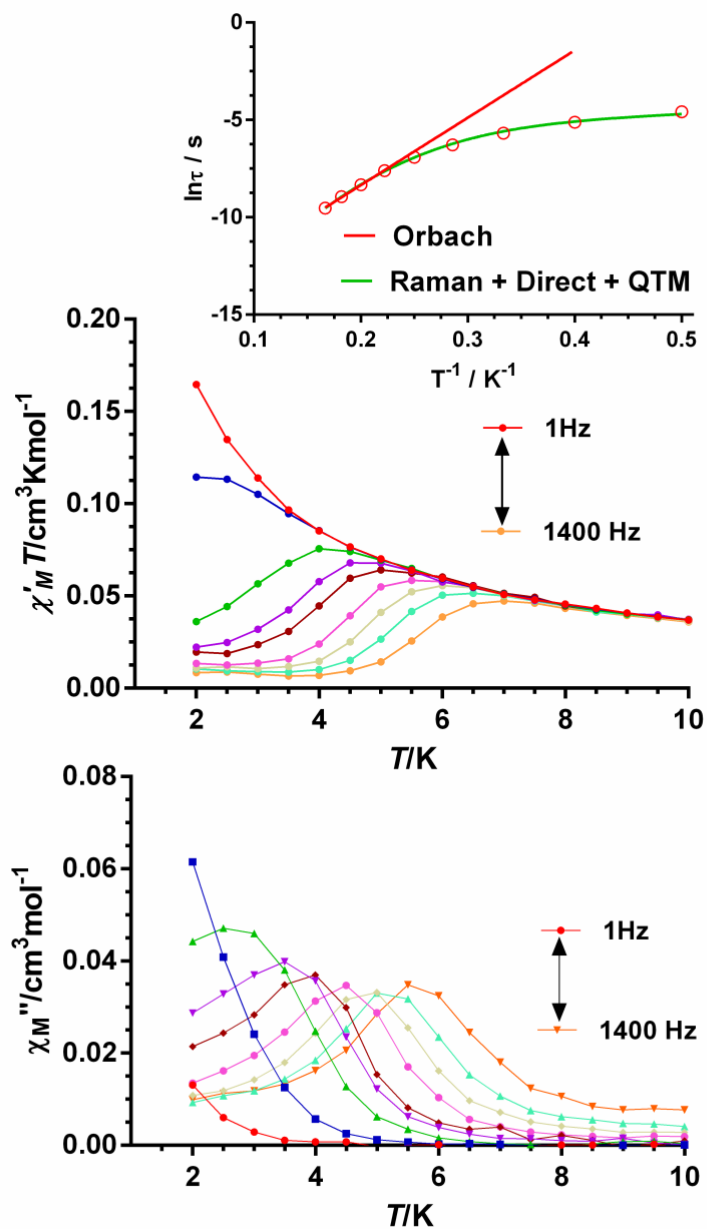


Figure 7. Temperature dependence of the in-phase (middle) and out-of-phase components (bottom) of the ac susceptibility at different frequencies  $2'$  (Dy/Y 1:10) measured under a 1000 Oe applied dc field. Solid lines are only guides for the eyes. Arrhenius plot (top inset). The green line represents the best fit to a direct plus Raman relaxation process.

As indicated elsewhere, theoretical calculations have shown that six-coordinated Co(II) complexes with trigonal prismatic and octahedral geometries should exhibit  $D < 0$  and  $D > 0$  values, respectively.<sup>11a</sup> Experimental results confirm these calculations, as all the Co(II) based SIMs with distorted octahedral geometries reported so far exhibit invariably positive values of the magnetic anisotropy (Table S5). It should be noted that  $D$  and  $E$  values derived from magnetization and susceptibility data are usually not very accurate because either the Hamiltonian used to model the data is not appropriate (ZFS with effective  $S = 3/2$  model is often used for complexes with actual first order SOC) or  $D$  is too high as to use the temperature dependence of magnetization vs field plots to extract accurate magnetic anisotropy parameters. Moreover, in some cases negative and positive  $D$  values lead to similar quality fits of the magnetic data. Therefore, to know the magnitude and sign of  $D$  in six-coordinated Co(II) based SIMs it is mandatory to combine several techniques. Thus, besides dc magnetic measurements (easier to access), direct techniques to determine the magnitude of  $\delta$ , such as inelastic neutron diffraction (INS) and FD-FT THz-EPR MDS spectroscopy, as well as HFEPR to find out the sign of  $D$  and the  $E/D$  ratio should be used. Theoretical calculations can be exploited to support experimental results. As can be observed in Table S5 this protocol, including direct techniques, has been only employed for complexes [Co( $\mu$ -L)( $\mu$ -OAc)(NO<sub>3</sub>)<sub>2</sub>] and **3**. If direct techniques for extracting the magnitude of  $\delta$  could not be used because of their limited access, then a combination of magnetic, HFEPR and theoretical calculations would be obligatory to achieve reliable values of  $D$  and  $E$ . Finally, it would be advisable in all cases to use magnetic diluted complexes to eventually suppress intermolecular magnetic interactions, which could partly or fully quench slow relaxation of the magnetization and therefore to hide the SIM behaviour.



**Figure 8.** Temperature dependence of the in-phase (middle) and out-of-phase components (bottom) of the ac susceptibility at different frequencies **3'** (Dy/Y 1:10) measured under a 1000 Oe applied dc field. Solid lines are only guides for the eyes. Arrhenius plot (top inset). The green line represents the best fit to a direct plus Raman relaxation process.

#### Acknowledgements

Financial support from Ministerio de Economía y Competitividad (MINECO) for Project CTQ2014-56312-P, the Junta de Andalucía (FQM-195 and the Project of excellence P11-FQM-7756), the University of Granada. M.A. P. thanks to MINECO for a Juan de la Cierva Incorporation contract (IJCI-2014-19485). J.N. acknowledge the Deutsche Forschungsgemeinschaft for a Research Fellowship (grant no. NE 2064/1-1 FOR).

## References

1.-(a) *Molecular Nanomagnets* Gatteschi, D.; Sessoli, R.; Villain, J.; Oxford University Press, Oxford, **2006**. (b) *Molecular Magnets: Physics and Applications*, Ed. Bartolomé, J.; Luis, F.; Fernández, J. F.; Springer-Verlag, Berlin-Heidelberg, **2014**. (c) *Molecular Nanomagnets and Related Phenomena*, Ed. Gao, S.; *Structure and Bonding*, Springer-Verlag, Berlin-Heidelberg, vol. 164, **2015**.

2.- (a) Bogani L.; Wernsdorfer, W.; Molecular spintronics using single-molecule magnets. *Nat. Mat.*, 2008, 7, 179-186; (b) Vincent, R.; Klyatskaya, S.; Ruben, M.; Wernsdorfer, W.; Balestro, F.; Electronic read-out of a single nuclear spin using a molecular spin transistor. *Nature*, 2012, 488, 357-360; (c) Ganzhorn, M.; Klyatskaya, S.; Ruben, M.; Wernsdorfer, W.; Strong spin-phonon coupling between a single-molecule magnet and a carbon nanotube nanoelectromechanical system. *Nature Nanotech.*, 2013, 8, 165-169; (d) Jenkins, M.; Hümmer, T.; Martínez-Pérez, M. J.; García-Ripoll, J.; Zueco D.; F. Luis, F.; Coupling single-molecule magnets to quantum circuits. *New. J. Physics*, 2013, 15, 095007. (e) Dediu, V. A.; Hueso, L. E.; Bergenti I.; Taliani, C.; Spin routes in organic semiconductors. *Nat. Mater.*, 2009, 8, 707-716. (f) Prezioso, M.; Riminucci, A.; Graziosi, P.; Bergenti, I.; Rakshit, R.; Cecchini, R.; Vianelli, A.; F. Borgatti, F.; Haag, N.; Willis, M.; Drew, A. J.; Gillin W. P.; Dediu, V. A.; A Single-Device Universal Logic Gate Based on a Magnetically Enhanced Memristor. *Adv. Mater.*, 2013, 25, 534-538. (g) Mannini, M.; Pineider, F.; Danieli, C.; Totti, F.; Sorace, L.; Sainctavit, Ph.; Arrio, M. A.; Otero, E.; Joly, L.; Cezar, J. C.; Cornia A.; Sessoli, R.; Quantum tunnelling of the magnetization in a monolayer of oriented single-molecule magnets. *Nature*, 2010, 468, 417-421. (h) Thiele, S.; Balestro, F.; Ballou, R.; Klyatskaya, S.; Ruben, M.; Wernsdorfer, W.; Electrically driven nuclear spin resonance in single-molecule magnets. *Science* 2014, 344, 1135-1138.

3.-(a) Rocha, A. R.; García-Suárez, V. M.; Bailey, S. W.; Lambert, C. J.; Ferrerand J.; Sanvito, S.; Towards molecular spintronics. *Nat. Mater.*, 2005, 4, 335-339; (b) Affronte, M.; Molecular Nanomagnets for information technologies. *J. Mater. Chem.*, 2009, 19, 1731-1737.

4.-R. Sessoli, R. ;Boulon, M. E. ;Caneschi, A ;Mannini, M ; Poggini, L. ; Wilhelm, F ; Rogalev, A. ; Strong magneto-chiral dichroism in a paramagnetic molecular helix observed by hard X-rays. *Nat. Phys.*, 2015,11, 69-74.

5.-(a) Leuenberger M. N.; Loss, D.; Quantum computing in molecular magnets.*Nature*, 2001, 410, 789-793; (b) Ardavan, A.; Rival, O.; Morton, J. J. L.; Blundell, S. J.;Tyryshkin, A. M.;Timco, G. A.;Winpenny, R. P. A.;Will Spin-Relaxation Times in Molecular Magnets Permit Quantum Information Processing?*Phys. Rev. Lett.*, 2007, 98, 057201; (c) Stamp P. C. E.;Gaita-Ariño, A.;Spin-based quantum computers made by chemistry: hows and whys.*J. Mater. Chem.*, 2009, 19, 1718-1730; (d) Martínez-Pérez, M. J.; Cardona-Serra, S.; Schlegel, C.; Moro, F.; Alonso, P.J.; Prima-García, H.; Clemente-Juan, J. M.;Evangelisti, M.;Gaita-Ariño, A.;Sesé, J.; Van Slageren, J.; Coronado E.; Luis, F.;Gd-Based Single-Ion Magnets with Tunable Magnetic Anisotropy: Molecular Design of Spin Qubits.*Phys. Rev. Lett.*, 2012, 108, 247213.

6.-Ayuk, M. A.; Hewitt, I. J.;Mareacre, V.;Clérac, R.; Wernsdorfer, W.; Anson, C.; Powell, A. K.;A Ferromagnetically Coupled Mn<sub>19</sub> Aggregate with a Record S=83/2 Ground Spin State. *Angew. Chem. Int. Ed.* 2006, 45, 4926 – 4929.

7.-a) Neese, F.;Pantazis, D. A.;What is not required to make a single molecule magnet. *Faraday Discuss.*, 2011, 148, 229-238; b)Waldmann, O.;A Criterion for the Anisotropy Barrier in Single-Molecule Magnets.*Inorg. Chem.* 2007, 46, 10035-10037.

8.- a) Tang, J.; Zhang, P; Lanthanide Single Molecule Magnets, Springer-Verlag Berlin Heidelberg 2015.(b) Frost, J. M.; Harriman, K. L. M.; Murugesu, M. The rise of 3-d single-ion magnets in molecular magnetism: towards materials from molecules? *Chem. Sci.* 2016, 7, 2470–2491. (c) Bar, A. K.; Pichon, C.; Sutter, J.-P.; Magnetic anisotropy in two- to eight-coordinated transition–metal complexes: Recent developments in molecular magnetism. *Coord. Chem. Rev.* 2016, 308, 346–380. (d) Craig, G. A.; Murrie, M. 3d single-ion magnets. *Chem. Soc. Rev.* 2015, 44, 2135– 2147. (e) Gómez-

Coca, S.; Aravena, D.; Morales, R.; Ruiz, E.; Large magnetic anisotropy in mononuclear metal complexes. *Coord. Chem. Rev.* 2015, 289-290, 379–392.

9.- Gómez-Coca, S.; Urtizberea, A.; Cremades, E.; Alonso, P. J.; Camón, A.; Ruiz, E.; Luis, F. Origin of slow magnetic relaxation in Kramers ions with non-uniaxial anisotropy. *Nat. Commun.* 2014, 5, 4300

10.- Colacio, E.; Ruiz, J.; Ruiz, E.; Cremades, E.; Krzystek, J.; Carretta, S.; Cano, J.; Guidi, T.; Wernsdorfer, W.; Brechin, E. K. Slow magnetic relaxation in a Co(II)-Y(III) single-ion magnet with positive axial zero-field splitting. *Angew. Chem., Int. Ed.* 2013, 52, 9130–9134.

11.- (a) Gómez-Coca, S.; Cremades, E.; Aliaga-Alcalde, N.; Ruiz, E. Mononuclear single-molecule magnets: Tailoring the magnetic anisotropy of first-row transition-metal complexes. *J. Am. Chem. Soc.* 2013, 135, 7010–7018, (b) Zhang, Y.-Z., Gómez-Coca, S., Brown, A. J., Saber, M. R., Zhang, X., Dunbar, K. R. Trigonal antiprismatic Co(II) single molecule magnets with large uniaxial anisotropies: importance of Raman and tunneling mechanisms, *Chem. Sci.*, 2016, 7, 6519-6527. (c) Pavlov, Alexander A.; Nelyubina, Yulia V.; Kats, Svitlana V.; Penkova, Larysa V.; Efimov, Nikolay N.; Dmitrienko, Artem O.; Vologzhanina, Anna V.; Belov, Alexander S.; Voloshin, Yan Z.; Novikov, Valentin V.; Polymorphism in a Cobalt-Based Single-Ion Magnet Tuning Its Barrier to Magnetization Relaxation, *J. Phys. Chem. Lett.* 2016, 7, 4111–4116, (d) Novikov, V. V.; Pavlov, A. A.; Nelyubina, Y. V.; Boulon, M.-E.; Varzatskii, O. A.; Voloshin, Y. Z.; Winpenny, R. E. P. A Trigonal Prismatic Mononuclear Cobalt(II) Complex Showing Single-Molecule Magnet Behavior. *J. Am. Chem. Soc.* 2015, 137, 9792–9795. (e) Zhu, Yaun-Yuan; Zhang, Yi-Quan; Yin, Ting-Ting; Gao, Chen; Wang, Bing-Wu; Gao, Song; A Family of CoII/CoIII Single-Ion Magnets with Zero-Field

SlowMagnetic Relaxation: Fine Tuning of Energy Barrier by Remote Substituent and Counter Cation, *Inorg. Chem.* 2015, 54, 5475–5486.

12.- (a) Sheng Zhang, Xiangyu Liu, Bin Liu, Zhengqiang Xia, Weitao Wang, Qi Yang, Hongshan Ke, Qing Wei, Gang Xie, Sanping Chen, Shengli Gao, 3D Co(II, III) mixed-valence metal-organic framework affording field-induced slow magnetic relaxation. *Sci. China. Chem.*, 2015, 58, 1032–1038. (b) Świtlicka-Olszewska, A.; Palion-Gazda, J.; Klemens, T.; Machura, B.; Vallejo, J.; Cano, J.; Lloret, F.; Julve, M. Single-ion magnet behaviour in mononuclear and two-dimensional dicyanamide-containing cobalt(II) complexes. *Dalton Trans.* 2016, 45, 10181–10193. (c) Vallejo, J.; Castro, I.; Ruiz-García, R.; Cano, J.; Julve, M.; Lloret, F.; De Munno, G.; Wernsdorfer, W.; Pardo, E. Field-induced slow magnetic relaxation in a six-coordinate mononuclear cobalt(II) complex with a positive anisotropy. *J. Am. Chem. Soc.* 2012, 134, 15704–15707. (d) Palion-Gazda, J.; Klemens, T.; Machura, B.; Vallejo, J.; Lloret, F.; Julve, M. Single ion magnet behaviour in a two-dimensional network of dicyanamide-bridged cobalt(II) ions. *Dalton Trans.* 2015, 44, 2989–2992. (e) Vallejo, Julia; Fortea-Pérez, Francisco R.; Pardo, Emilio; Benmansour, Samia; Castro, Isabel; Krzystek, J.; Armentano, Donatella; Cano, Joan; Guest-dependent single-ion magnet behaviour in a cobalt(II) metal-organic framework, *Chem. Sci.*, 2016, 7, 2286–2293. (f) Zhu, Y. Y.; Zhu, M. S.; Yin, T. T.; Meng, Y. S.; Wu, Z. Q.; Zhang, Y. Q.; Gao, S. Cobalt(II) coordination polymer exhibiting single-ion magnet-type field-induced slow relaxation behavior. *Inorg. Chem.* 2015, 54, 3716–3718. (g) Nedelko, N.; Kornowicz, A.; Justyniak, I.; Aleshkevych, P.; Prochowicz, D.; Krupiński, P.; Dorosh, O.; Ślawska-Waniewska, A.; Lewiński, J. Supramolecular Control over Molecular Magnetic Materials:  $\gamma$ -Cyclodextrin-Templated Grid of Cobalt(II) Single-Ion Magnets. *Inorg. Chem.* 2014, 53, 12870–12876. (h) Ion, A. E.; Nica, S.; Madalan, A. M.; Shova, S.; Vallejo, J.; Julve, M.; Lloret, F.; Andruh, M. Two-Dimensional Coordination Polymers Constructed Using, Simultaneously, Linear and Angular Spacers and Cobalt(II) Nodes. New Examples of Networks of Single-Ion Magnets. *Inorg. Chem.* 2015, 54, 16–18. (i) Wang, Yu-Ling; Chen, Lin; Liu, Cai-Ming; Zhang, Yi-Quan; Yin, Shun-Gao; Liu, Qing-Yan; Field-Induced Slow Magnetic Relaxation and Gas Adsorption Properties of a Bifunctional Cobalt(II) Compound, *Inorg. Chem.* 2015, 54, 11362–11368. (j) Zhu, Y.-Y.; Yin, T.-T.; Liu, C.-W.; Gao, C.; Wu, Z.-Q.; Zhang, Y.-Q.; Wang, B.-W.; Gao, S. Field-induced

slow magnetic relaxation in a hydrogen-bonding linked Co(II) 1D supramolecular coordination polymer. *Supramol. Chem.* 2015, 27, 401–406. (k) Mondal, Amit Kumar; Khatua, Sajal; Tomar, Kapil; Konar, Sanjit; Field-Induced Single-Ion-Magnetic Behavior of Octahedral Co(II) in a Two-Dimensional Coordination Polymer. *Eur. J. Inorg. Chem.* 2016, 3545–3552. (l) Wu, D.; Zhang, X.; Huang, P.; Huang, W.; Ruan, M.; Ouyang, Z. W. Tuning transverse anisotropy in Co(III)–Co(II)–Co(III) mixed-valence complex toward slow magnetic relaxation. *Inorg. Chem.* 2013, 52, 10976–10982. (m) Herchel, R.; Váhovská, L.; Potočňák, I.; Trávníček, Z. Slow Magnetic Relaxation in octahedral cobalt(II) field-induced single-ion magnet with positive axial and large rhombic anisotropy. *Inorg. Chem.* 2014, 53, 5896–5898. (n) Zhu, Y. Y.; Zhu, M. S.; Yin, T. T.; Meng, Y. S.; Wu, Z. Q.; Zhang, Y. Q.; Gao, S. Cobalt(II) coordination polymer exhibiting single-ion magnet-type field-induced slow relaxation behavior. *Inorg. Chem.* 2015, 54, 3716–3718. (o) Walsh, J. P. S.; Bowling, G.; Ariciu, A.-M.; Jailani, N. F. M.; Chilton, N. F.; Waddell, P. G.; Collison, D.; Tuna, F.; Higham, L. J. Evidence of slow magnetic relaxation in  $\text{Co}(\text{AcO})_2(\text{py})_2(\text{H}_2\text{O})_2$ . *Magnetochemistry* 2016, 2, 23–33. (p) Tong, Jin; Demeshko, Serhiy; John, Michael; Dechert, Sebastian; Meyer, Franc; Redox-Induced Single-Molecule Magnetism in Mixed-Valent  $[2 \times 2]$   $\text{Co}_4$  Grid Complexes, *Inorg. Chem.* 2016, 55, 4362–4372. (q) Plenk, C.; Krause, J.; Rentschler, E. A click-functionalized single-molecule magnet based on cobalt(II) and its analogous manganese(II) and zinc(II) compounds. *Eur. J. Inorg. Chem.* 2015, 2015, 370–374. (r) Liu, X.; Sun, L.; Zhou, H.; Cen, P.; Jin, X.; Xie, G.; Chen, S.; Hu, Q. Single-ion-magnet behavior in a two-dimensional coordination polymer constructed from Co(II) nodes and a pyridylhydrazone derivative. *Inorg. Chem.* 2015, 54, 8884–8886. (s) Wu, D.-Y.; Zhang, X.-X.; Huang, P.; Huang, W.; Ruan, M.-Y.; Ouyang, Z. W. Tuning Transverse Anisotropy in Co(III)–Co(II)–Co(III) Mixed-Valence Complex toward Slow Magnetic Relaxation. *Inorg. Chem.* 2013, 52, 10976–10982. (t) Chandrasekhar, Vadapalli; Dey, Atanu; Mota, Antonio J.; Colacio, Enrique; Slow Magnetic Relaxation in Co(III)–Co(II) Mixed-Valence Dinuclear Complexes with a  $\text{Co}(\text{IO}_5\text{X})$  ( $\text{X} = \text{Cl}, \text{Br}, \text{NO}_3$ ) Distorted-Octahedral Coordination Sphere, *Inorg. Chem.* 2013, 52, 4554–4561. (u) Díaz-Torres, R.; Menelaou, M.; Roubeau, O.; Sorrenti, A.; Brandariz-de-Pedro, G.; Sañudo, E. C.; Teat, S. J.; Fraxedas, J.; Ruiz, E.; Aliaga-Alcalde, N.; Multiscale study of mononuclear Co(II) SMMs based on curcuminoid ligands *Chem. Sci.*, 2016, 7, 2793–2803. (v) Roy, Subhadip; Oyarzabal, Itziar; Vallejo, Julia; Cano, Joan; Colacio,

Enrique;Bauza, Antonio;Frontera, Antonio;Kirillov, Alexander M.;Drew, Michael G. B.;Das, Subrata;Two Polymorphic Forms of a Six-Coordinate Mononuclear Cobalt(II) Complex with Easy-plane Anisotropy: Structural Features, Theoretical Calculations, and Field-Induced Slow Relaxation of the Magnetization, *Inorg. Chem.* 2016, 55, 8502–8513

13.- Colacio, E.; Ruiz, J.; Mota, A. J.; Palacios, M. A.; Cremades, E.; Ruiz, E.; White, F. J.; Brechin, E. K.; Family of Carboxylate- and Nitrate diphenoxo Triply Bridged DinuclearNiIIInIII Complexes (Ln = Eu, Gd, Tb, Ho, Er, Y): Synthesis, Experimental and Theoretical Magneto-Structural Studies, and Single-Molecule Magnet Behavior*Inorg. Chem.***2012**, 51, 5857-5868.

14.- Hassan, A. K.; Pardi, L. A.; Krzystek, J.; Sienkiewicz, A.; Goy, P.;Rohrer, M.; Brunel, L. C. Ultrawide band multifrequency high-fieldEMR technique: A methodology for increasing spectroscopic information. *J. Magn. Reson.* 2000, 142, 300.

15.- Schnegg, A.; Behrends, J.; Lips, K.; Bittl, R.; Holldack, K., Frequency domain Fourier transform THz-EPR on single molecule magnets using coherent synchrotron radiation. *Phys. Chem. Chem. Phys.* **2009**,11 (31), 6820-6825.

16.- Nehr Korn, J.; Martins, B. M.; Holldack, K.; Stoll, S.; Dobbek, H.; Bittl, R.; Schnegg, A., Zero-field splittings in metHb and metMb with aquo and fluoro ligands: a FD-FTTHz-EPR study. *Mol. Phys.* **2013**,111 (18-19), 2696-2707.

17.- bo-Bakr, M.; Feikes, J.; Holldack, K.; Kuske, P.; Peatman, W. B.; Schade, U.; Wüstefeld, G.; Hübers, H. W., Brilliant, Coherent Far-Infrared (THz) Synchrotron Radiation. *Phys. Rev. Lett.* **2003**,90 (9), 094801.

18.- Stoll, S.; Schweiger, A., EasySpin, a comprehensive software package for spectral simulation and analysis in EPR. *J. Magn. Reson.* **2006**,178 (1), 42-55.

19.- (a) Nehr Korn, J.; Schnegg, A.; Holldack, K.; Stoll, S., General Magnetic Transition Dipole Moments for Electron Paramagnetic Resonance. *Phys. Rev. Lett.* **2015**,114 (1), 010801.(b) Nehr Korn, J.; Telser, J.; Holldack, K.; Stoll, S.; Schnegg, A., Simulating Frequency-Domain Electron Paramagnetic Resonance: Bridging the Gap between

Experiment and Magnetic Parameters for High-Spin Transition-Metal Ion Complexes.

*J. Phys. Chem. B* **2015**, *119* (43), 13816-13824.

20.- APEX2; Bruker AXS: Madison, WI, 2010.

21.- SAINT, Version 8.30a; Bruker AXS: Madison, WI, 2013.

22.-Sheldrick, G. M. SADABS, Version 2004/1; Bruker AXS:Madison, WI, 2008.

23.-CrysAlisPro Software System. Agilent Technologies UK Ltd. Oxford, UK, 2012.

24.-Sheldrick, G.M. SHELXL-97. A Program for Crystal Structure

Refinement.University of Göttingen, Germany, 1997. SHELXTL Version 2014/7.

<http://shelx.uni-ac.gwdg.de/SHELX/index.php>.

25.- (a) Karlstroem, G.; Lindh, R.; Malmqvist, P.-A.; Roos, B. O.;Ryde, U.; Veryazov, V.; Widmark, P.-O.; Cossi, M.; Schimmelpfennig,B.; Neogrady, P.; Seijo, L. MOLCAS: a program package forcomputational chemistry. *Comput. Mater. Sci.* 2003, 28, 222–239. (b) Veryazov, V.; Widmark, P.-O.; SerranoAndres, L.; Lindh, R.; Roos, B. O. 2MOLCAS as a development platform for quantum chemistry software. *Int. J. Quantum Chem.* 2004, 100, 626–635. (c) Aquilante, F.; De Vico, L.; Ferre, N.; Ghigo, G.; Malmqvist, P.-a.; Neogrady, P.; Pedersen, T. B.; Pitonak, M.; Reiher, M.; Roos, B. O.; Serrano-Andres, L.; Urban, M.; Veryazov, V.; Lindh, R. MOLCAS 7:The Next Generation. *J. Comput. Chem.* 2010, 31, 224–247. (d) Duncan, J. A. Molcas 7.2. *J. Am. Chem. Soc.* 2009, 131 (6), 2416.

26.- (a) Neese, F.; Petrenko, T.; Ganyushin, D.; Olbrich, G. Advanced aspects of ab initio theoretical optical spectroscopy of transition metal complexes: Multiplets, spin-orbit coupling andresonance Raman intensities. *Coord. Chem. Rev.* 2007, 251, 288–327. (b) Neese, F. The ORCA program system. *Wiley Interdisciplinary Reviews-Computational Molecular Science* 2012, 2, 73–78. (c) Neese, F.ORCA; University of Bonn: Bonn, Germany, 2010.

27.-Chibotaru, L. F.; Ungur, L. Ab initio calculation of anisotropic magnetic properties of complexes. I. Unique definition of pseudo spin Hamiltonians and their derivation. *J. Chem. Phys.* 2012, 137, 064112.

28.- (a) Roos, B. O.; Veryazov V.; Widmark, P. O.; *Theor. Chim. Acta.*, **2004**, 111, 345; (b) Roos, B. O.; Lindh, R.; Malmqvist, P. A.; Veryazov V.; Widmark, P. O.; Main Group Atoms and Dimers Studied with a New Relativistic ANO Basis Set. *J. Phys. Chem. A*, **2004**, 108, 2851-2858; (c) Roos, B. O.; Lindh, R.; Malmqvist, P. A.; Veryazov V.; Widmark, P. O.; New Relativistic ANO Basis Sets for Transition Metal Atoms. *J. Phys. Chem. A*, **2005**, 109, 6575-6579; (d) Roos, B. O.; Lindh, R.; Malmqvist, P. A.; Veryazov, V.; Widmark, P. O.; New relativistic ANO basis sets for actinide atoms. *Chem. Phys. Letters*, **2005**, 409, 295-299.

29.- (a) Ganyushin, D.; Neese, F., A fully variational spin-orbit coupled complete active space self-consistent field approach: Application to electron paramagnetic resonance g-tensors. *The Journal of Chemical Physics* **2013**, 138 (10), 104113. (b) Ganyushin, D.; Neese, F. First-principles calculations of zero-field splitting parameters. *J. Chem. Phys.* 2006, 125, 024103. (c) Maurice, R.; Bastardis, R.; Graaf, C. d.; Suaud, N.; Mallah, T.; Guihéry, N., Universal Theoretical Approach to Extract Anisotropic Spin Hamiltonians. *Journal of Chemical Theory and Computation* **2009**, 5 (11), 2977-2984.

30.- (a) Angeli, C.; Cimiraglia, R.; Evangelisti, S.; Leininger, T.; Malrieu, J. P. Introduction of n-electron valence states for multireference perturbation theory. *J. Chem. Phys.* 2001, 114, 10252-10264. (b) Angeli, C.; Cimiraglia, R.; Malrieu, J.-P. N-electron valence state perturbation theory: a fast implementation of the strongly contracted variant. *Chem. Phys. Lett.* 2001, 350, 297-305. (c) Angeli, C.; Cimiraglia, R. Multireference perturbation configuration interaction V. Third-order energy contributions in the Moller-Plesset and Epstein-Nesbet partitions. *Theor. Chem. Acc.* 2002, 107, 313-317. (d) Angeli, C.; Cimiraglia, R.; Malrieu, J.-P. n-electron valence state perturbation theory: a spinless formulation and an efficient implementation of

the strongly contracted and of the partially contracted variants. *J. Chem. Phys.* 2002, 117, 9138–9153.

31.- Douglas, M.; Kroll, N. M., Quantum electrodynamical corrections to the fine structure of helium. *Annals of Physics* **1974**, 82 (1), 89-155.

32.- (a) Weigend, F.; Ahlrichs, R. Balanced basis sets of split valence, triple zeta valence and quadruple zeta valence quality for H to Rn: Design and assessment of accuracy. *Phys. Chem. Chem. Phys.* 2005, 7, 3297–3305. (b) Schaefer, A.; Horn, H.; Ahlrichs, R. Fully optimized contracted Gaussian basis sets for atoms Li to Kr. *J. Chem. Phys.* 1992, 97, 2571–2577. (c) Schaefer, A.; Huber, C.; Ahlrichs, R. Fully optimized contracted Gaussian basis sets of triple zeta valence quality for atoms Li to Kr. *J. Chem. Phys.* 1994, 100, 5829–5835. (d) Schäfer, A.; Huber, C.; Ahlrichs, R., Fully optimized contracted Gaussian basis sets of triple zeta valence quality for atoms Li to Kr. *The Journal of Chemical Physics* **1994**, 100 (8), 5829-5835.

33.-Atanasov, M.; Ganyushin, D.; Sivalingam, K.; Neese, F., A Modern First-Principles View on Ligand Field Theory Through the Eyes of Correlated Multireference Wavefunctions. In *Molecular Electronic Structures of Transition Metal Complexes II*, Mingos, P. D. M.; Day, P.; Dahl, P. J., Eds. Springer Berlin Heidelberg: Berlin, Heidelberg, 2012; pp 149-220.

34.- Titos-Padilla, S., Ruiz, J., Herrera, J.M., Brechin, E.K., Wersndorfer, W. Lloret, F., Colacio E., Family of Carboxylate- and Nitrate-diphenoxo Triply Bridged Dinuclear Ni(II)Ln(III) Complexes (Ln = Eu, Gd, Tb, Ho, Er, Y): Synthesis, Experimental and Theoretical Magneto-Structural Studies, and Single-Molecule Magnet Behavior, *Inorg. Chem.* **2013**, 52, 9620-6.

35.- Llunell, M.; Casanova, D.; Cirera, J.; Alemany, P.; Alvarez, S. SHAPE, version 2.0; Universitat de Barcelona: Barcelona, Spain, 2010.

- 36.- Chilton, N. F.; Anderson, R. P.; Turner, L. D.; Soncini, A.; Murray, K. S. A powerful new program for the analysis of anisotropic monomeric and exchange-coupled polynuclear d- and f-block complexes, *J. Comput. Chem.* 2013, 34, 1164–1175.
- 37.- Nehr Korn, Joscha; Veber, Sergey L.; Sutura, Elizaveta A.; Zhukas, Luidmilla; Fomina, Irina; Belov, Alexander; Colacio, Enrique; Palacios, M. A.; Brechin, Euan K.; Fursova, Elena V.; Cucos, Paula; Andruh, Marius; Krzystek, Jurek; Stoll, Stefan; Holldack Karsten; Schnegg, Alexander; Probing effective models for the magnetic properties of  $\text{Co}^{\text{II}}$  with large ZFS: Experimental and computational study. Submitted for publication.
- 38.- Abragam, A.; Bleaney, B. *Electron Paramagnetic Resonance of Transition Ions*, Clarendon Press. Oxford, **1970**.
- 39.- Singh, A.; Shrivastava, K. Optical-acoustic two-phonon relaxation in spin systems, *Phys. Status Solidi B* 1979, 95, 273. Shrivastava, K. N., Theory of Spin-Lattice Relaxation *Phys. Status Solidi B*, 1983, 117, 437–458.
- 40.- a) Vaidya S., Tewary, S., Kumar Singh, S., Langley, S. K., Murray, K. S. Lan, Y., Wernsdorfer W.; Rajaraman G.; Shanmugam M. What Controls the Sign and Magnitude of Magnetic Anisotropy in Tetrahedral Cobalt(II) Single-Ion Magnets? ; *Inorg. Chem.* 2016, 55, 9564-9578. b) Ishikawa, R.; Horii, Y., Nakanishi, R.; Ueno, S., Breedlove, B. K., Yamashita, M., Kawata S.; *Eur. J. Inorg. Chem.* 3233-3239. S. Sottini, G. Poneti, S. Ciattini, N. Levesanos, E. Ferentinos, J. Krzystek, L. Sorace, P. Kyritsis Field-Induced Single-Ion Magnetism Based on Spin-Phonon Relaxation in a Distorted Octahedral High-Spin Cobalt(II) Complex c) Magnetic Anisotropy of Tetrahedral  $\text{Co}^{\text{II}}$  Single-Ion Magnets: Solid-State Effects, *Inorg. Chem.* 2016, 55, 9537–9548 d) F. Habib, I. Korobkov, M. Murugesu Exposing the intermolecular nature of the second relaxation pathway in a mononuclear cobalt(II) single-molecule magnet with positive

anisotropy, *Dalton Trans.*, 2015, 44, 6368-6373. e) J. Li, Y. Han, F. Cao, R.-M. Wei, Y.-Q. Zhang, Y. Song Two field-induced slow magnetic relaxation processes in a mononuclear Co(II) complex with a distorted octahedral geometry, *Dalton Trans.*, 2016, 45, 9279.